The cephalic phase of insulin release is modulated by IL-1β

Sophia J. Wiedemann, Kelly Trimigliozzi, Erez Dror, Daniel T. Meier, Jose Alberto Molina-Tijeras, Leila Rachid, Christelle Le Foll, Christophe Magnan, Friederike Schulze, Marc Stawiski, et al.

Cell Metabolism

Article

The cephalic phase of insulin release is modulated by IL-1β

Graphical abstract

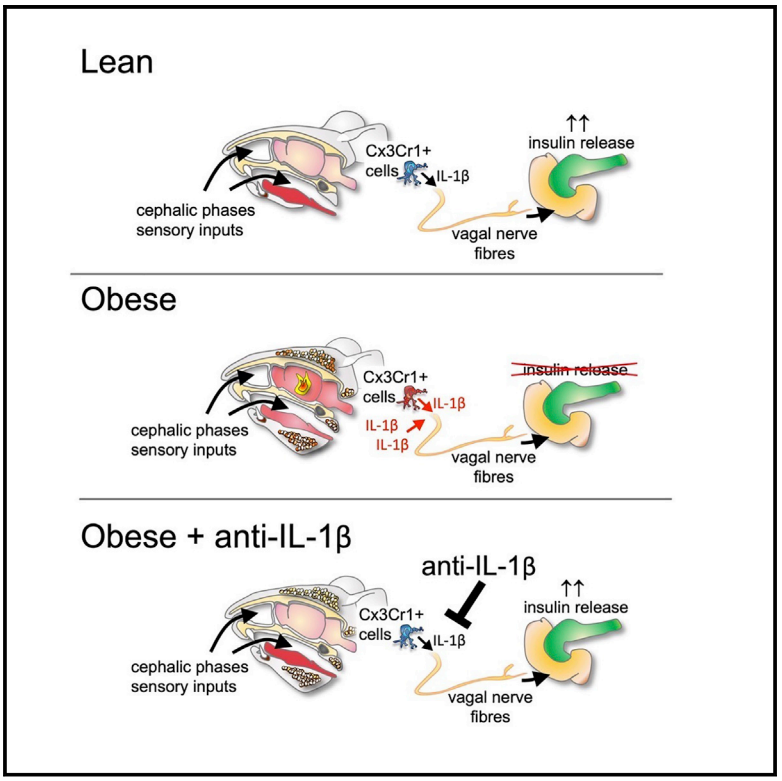

Highlights

- IL-1β stimulates insulin secretion via neuronal transmission
- IL-1β mediates the cephalic phase of insulin release
- IL-1β derived from microglia facilitates cephalic phase insulin release
- In obesity, dysfunctional IL-1β signaling impairs cephalic phase insulin release

Authors

Sophia J. Wiedemann,
Kelly Trimigliozzi, Erez Dror, ...,
Hélène Méreau,
Marianne Böni-Schnetzler,
Marc Y. Donath

Correspondence

sophia.j.wiedemann@gmail.com

In brief

Wiedemann et al. demonstrate that IL-1β stimulates insulin secretion via neuronal transmission and that blocking IL-1β suppresses the cephalic phase insulin response. Microglia are the source of IL-1β in cephalic phase insulin release. Dysregulated IL-1β signaling during obesity results in impaired cephalic phase insulin secretion.

Wiedemann et al., 2022, Cell Metabolism *34*, 991–1003
July 5, 2022
https://doi.org/10.1016/j.cmet.2022.06.001

CellPress

Cell Metabolism

CellPress
OPEN ACCESS

Article

The cephalic phase of insulin release is modulated by IL-1β

Sophia J. Wiedemann,[1,2,5,6,*] Kelly Trimigliozzi,[1,2,5] Erez Dror,[1,2] Daniel T. Meier,[1,2] Jose Alberto Molina-Tijeras,[1,2] Leila Rachid,[1,2] Christelle Le Foll,[3] Christophe Magnan,[4] Friederike Schulze,[1,2] Marc Stawiski,[1,2] Stéphanie P. Häuselmann,[1,2] Hélène Méreau,[1,2] Marianne Böni-Schnetzler,[1,2] and Marc Y. Donath[1,2]

[1]Clinic of Endocrinology, Diabetes and Metabolism University Hospital Basel, Basel, Switzerland
[2]Department of Biomedicine, University of Basel, Basel, Switzerland
[3]Institute of Veterinary Physiology, Vetsuisse Faculty, University of Zurich, Zurich, Switzerland
[4]Université de Paris, BFA, UMR 8251, CNRS, 75013 Paris, France
[5]These authors contributed equally
[6]Lead contact
*Correspondence: sophia.j.wiedemann@gmail.com
https://doi.org/10.1016/j.cmet.2022.06.001

SUMMARY

The initial cephalic phase of insulin secretion is mediated through the vagus nerve and is not due to glycemic stimulation of pancreatic β cells. Recently, IL-1β was shown to stimulate postprandial insulin secretion. Here, we describe that this incretin-like effect of IL-1β involves neuronal transmission. Furthermore, we found that cephalic phase insulin release was mediated by IL-1β originating from microglia. Moreover, IL-1β activated the vagus nerve to induce insulin secretion and regulated the activity of the hypothalamus in response to cephalic stimulation. Notably, cephalic phase insulin release was impaired in obesity, in both mice and humans, and in mice, this was due to dysregulated IL-1β signaling. Our findings attribute a regulatory role to IL-1β in the integration of nutrient-derived sensory information, subsequent neuronally mediated insulin secretion, and the dysregulation of autonomic cephalic phase responses in obesity.

INTRODUCTION

Insulin secretion is regulated by multiple factors. Although the direct effects of glucose acting on pancreatic β cells constitute the most prominent stimulus of insulin secretion (Röder et al., 2016; Sharpey-Schäfer, 1924), other mechanisms such as neuronal stimulation and incretin hormones may account for as much as 70%–80% of the total insulin response to a meal (Berthoud, 1984; Nauck et al., 1986).

Cephalic phase insulin release is the consequence of sensory stimuli from food (sight, smell, taste, proprioceptive, and tactile stimulation) acting on receptors in the head and oropharynx prior to the direct stimulatory effects of glucose on β cells (Berthoud et al., 1980; Powley, 1977). These stimuli then entail activation of the parasympathetic nervous system and downstream insulin secretion (Ahrén et al., 1990; Berthoud et al., 1981; Strubbe, 1992). Cephalic phase responses are essential in the postprandial regulation of glucose homeostasis because a meal that bypasses the oral cavity, and thus cephalic phase responses, causes glucose intolerance (Ahrén, 2000; Brede et al., 2020, 2017; Andersen et al., 1995; Lorentzen et al., 1987; Louis-Sylvestre, 1976; Steffens, 1976; Teff and Engelman, 1996). Apart from muscarinic receptor signaling in β cells and hypothalamic monoamines, no molecular mediator of cephalic phase insulin release has been described to date (Berthoud and Jeanrenaud, 1982; Holmes et al., 1989; Strubbe et al., 1987).

IL-1β regulates the organism's response to tissue damage and pathogens (Dinarello, 2013). More recently, IL-1β was shown to be an essential player in both the physiology and pathology of glucose metabolism (Bendtzen et al., 1986; Donath et al., 2019; Donath and Shoelson, 2011; Hajmrle et al., 2016; Larsen et al., 2007). Indeed, the chronic activation of IL-1β in patients with metabolic syndrome promotes β cell toxicity and ultimately failure—characteristic features of type 2 diabetes (Böni-Schnetzler et al., 2008; Maedler et al., 2002). In contrast to these deleterious long-term effects, acute food intake primes myeloid cells to produce IL-1β, which then contributes to the physiological postprandial stimulation of insulin secretion (Dror et al., 2017). However, the underlying mechanisms of this incretin-like effect of IL-1β on insulin release remain unknown.

We hypothesized that IL-1β exerts its secretagogue effect on insulin secretion via stimulation of the parasympathetic nervous system. Using genetic and pharmacological models, we found IL-1β to mediate its stimulatory effect on insulin secretion via central muscarinic signaling. In order to substantiate the neuronal involvement of IL-1β-mediated insulin release, we studied the cephalic phase insulin response as a prime example of centrally mediated insulin secretion. We identified IL1β as a crucial mediator of this cephalic phase reflex. Originating from long-lived CX3CR1+ myeloid cells, such as microglia, it regulated neuronal activity in the hypothalamus in response to cephalic stimulation. Notably, we found cephalic

phase insulin release to be impaired in obesity, in both mice and humans, in an IL-1β-dependent manner in mice. Thus, IL-1β has a regulatory role in the neuronal stimulation of insulin secretion and in the dysregulation of autonomic cephalic phase responses in obesity.

RESULTS

IL-1β-induced insulin secretion requires central muscarinic receptor signaling

First, we tested whether neuronal transmission is involved in IL-1β-induced insulin release. We confirmed (Dror et al., 2017) that the intraperitoneal (i.p.) injection of IL-1β, prior to an i.p. glucose tolerance test (GTT), strongly potentiated insulin secretion (Figures 1A and 1B) along with enhanced glucose clearance (Figures 1C and 1D). The muscarinic acetylcholine-receptor antagonist atropine strongly decreased the stimulation of insulin secretion by IL-1β (Figures 1A–1D), suggesting a role for neuronal transmission in IL-1β-induced insulin release. To further delineate the involvement of the nervous system in this setting, we compared pre-injections of two muscarinic acetylcholine-receptor antagonists that do not cross the blood-brain barrier with atropine, which penetrates the blood-brain barrier (Virtanen et al., 1982). In contrast to atropine, ipratropium bromide (no specificity for muscarinic receptor subtypes [Casarosa et al., 2009]) (Figures 1E–1H) and darifenacin (a specific muscarinic M3 receptor antagonist—the subtype also expressed in pancreatic islets [Duttaroy et al., 2004; Gautam et al., 2006; Zinner, 2007]) (Figures 1I–1L) were unable to block the IL-1β-induced effect on insulin secretion, pointing to a central neuronal effect. Both atropine and ipratropium bromide delayed gastric emptying, as shown by the pharmacokinetics of paracetamol absorption, indicating that the compounds and doses used in our study were effective (Figure S1A). Next, we compared the effect of i.p. versus intracerebroventricular (i.c.v.) administration of IL-1β. Mice that received IL-1β injections prior to the GTT directly into the cerebrospinal fluid reacted the same way as their i.p. injected counterparts, significantly improving glucose tolerance (Figures 1M–1P). Of note, when assessing serum IL-1β levels post injection, we found that both i.p. and i.c.v. injected mice showed significantly more IL-1β than control i.p. or i.c.v. injected mice (Figure S1B). To confirm that this was indeed through leakage of IL-1β into the systemic circulation and not via induction of endogenous IL-1β production in peripheral tissues, we i.c.v. injected IL-1β into IL-1β whole-body knockout (KO) mice ($Il1b^{-/-}$). $Il1b^{-/-}$ mice also had increased systemic IL-1β levels post i.c.v. injection of IL-1β, confirming leakage of the protein (Figures S1C–S1E). Further i.c.v. injections with a 10-fold lower concentration of IL-1β also resulted in elevated IL-1β levels in circulation (Figure S1F). However, mice that were treated with this 10-fold lower dose of IL-1β i.p. did not show altered insulin secretion or improved glucose tolerance when compared with control mice (Figures S1G and S1H). Furthermore, mice that received IL-1β by i.c.v. injection reached their peak of insulin secretion after 15 min (Figure 1M), whereas the peak of IL-1β measured systemically in the $Il1b^{-/-}$ mice was 30 min after injection (Figure S1C). This indicates that centrally administered IL-1β most likely exerts its insulin stimulatory effect before leaking into the periphery. Overall, these data show that IL-1β-induced insulin secretion requires central muscarinic receptor signaling.

Cephalic phase insulin release is mediated by IL-1β

To better dissect the precise role of neuronal transmission in IL-1β-induced insulin release, we investigated the neuronally mediated cephalic phase of insulin release. First, we developed a mouse model to study this phase of insulin secretion (Figure 2A; Video S1). Mice were fasted overnight and placed into a new cage containing either a single pellet of the chow they were accustomed to (cephalic condition) or no food (control condition). Cephalic-stimulated mice were then allowed to voluntarily approach the food pellet. Blood was sampled immediately after the first bite of food. This brief cephalic stimulation was sufficient to increase circulating insulin concentration (Figure 2B) in the complete absence of a rise in blood glucose (Figure 2C), confirming the validity of the model. To ensure that the observed insulin secretion was dependent on the food stimulus alone and not on the visual stimulus of a startling object, we repeated cephalic stimulation experiments with a non-edible object, a rubber stopper the shape and size of a pellet (Chen et al., 2015). In contrast to the food pellet, the non-edible object failed to increase insulin levels (Figures 2D and 2E). Thus, a realistic food stimulation is mandatory to elicit cephalic insulin secretion. Next, we assessed the functional importance of the cephalic phase stimulation on overall glucose tolerance. Cephalic-preconditioned mice showed increased total insulin release (Figures 2F and 2G) and improved glucose tolerance (Figures 2H and 2I) upon oral glucose load—emphasizing the importance of cephalic phase reflexes for early insulin secretion and glucose disposal following food intake. Interestingly, the intravenous administration of a low dose of exogenous insulin prior to an oral GTT did not result in improved glucose tolerance (Figures S2A and S2B). This demonstrates the important contribution of cephalic phase reflexes as a whole, rather than cephalic insulin secretion alone, to post-meal glucose homeostasis. We then assessed the importance of IL-1β in the cephalic phase of insulin secretion. Pre-injection of the IL-1 receptor type I antagonist IL-1Ra diminished cephalic phase insulin secretion (Figures 3A and 3B). Since the IL-1 receptor type I is the receptor for both IL-1β and IL-1α, we also used a neutralizing antibody specifically against mouse IL-1β (anti-IL-1β). Treatment with anti-IL-1β also inhibited cephalic phase insulin secretion (Figures 3C and 3D). Moreover, $Il1b^{-/-}$ mice also showed reduced insulin levels after cephalic stimulation compared with wild-type (WT) littermate controls (Figures 3E–3G). Therefore, the cephalic phase of insulin secretion is mediated by IL-1β.

Cephalic phase IL-1β originates from long-lived CX3CR1+ myeloid cells

Next, we evaluated the cellular source of IL-1β in cephalic phase insulin secretion. Following cephalic stimulation, serum IL-1β levels largely remained below the detection limit (Figure 4A), pointing toward local processes in the tissues rather than a systemic action of IL-1β. We then assessed whether IL-1β in the cephalic phase acts within the central nervous system (CNS). To do this, cephalic-stimulated WT mice received injections of IL-1Ra directly into the cerebral ventricular system. Animals injected i.c.v. showed reduced cephalic phase insulin release (Figures 4B and 4C). Of

CellPress
OPEN ACCESS

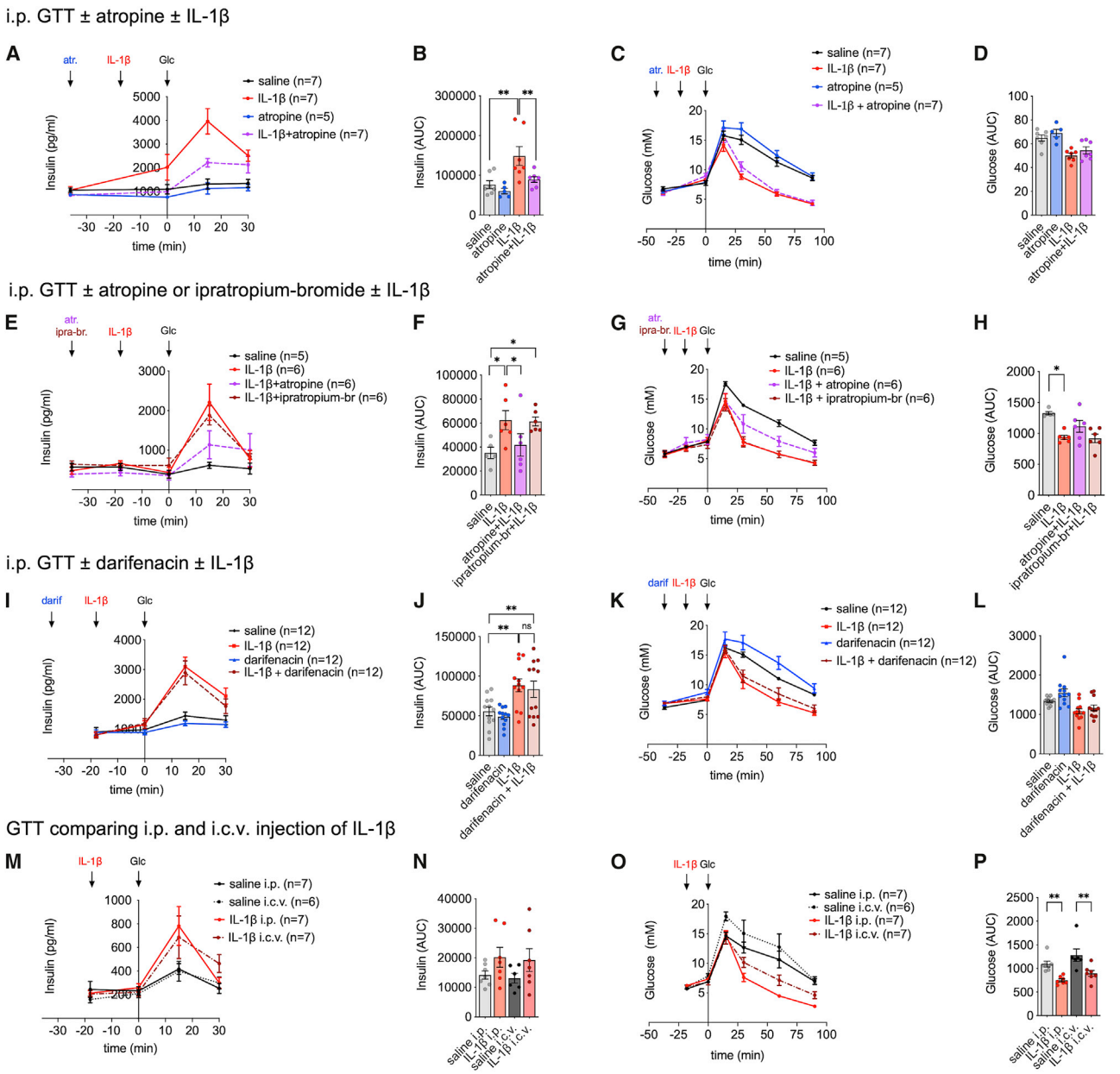

Figure 1. IL-1β-induced insulin secretion requires central muscarinic receptor signaling

(A–L) Male mice received three injections. First (T = −36 min): saline or specific treatment as indicated. Second (T = −18 min): saline or IL-1β (1 μg/kg BW). Third (T = 0 min) glucose (2 g/kg BW).

(A–D) Measurements during an i.p. GTT in atropine-treated (5 mg/kg BW) mice.

(E–H) Measurements during an i.p. GTT in ipratropium bromide-treated (7.2 mg/kg BW) mice.

(I–L) Measurements during an i.p. GTT in darifenacin-treated (5 mg/kg BW) mice.

(M–P) Measurements during a GTT in female mice that received two injections. First (T = −18 min): saline or IL-1β (1 μg/kg BW) either i.p. or i.c.v. Second i.p. injection (T= 0 min): glucose (2 g/kg BW).

Data are presented as individual measurements (points in B, D, F, H, J, L, N, and P) and arithmetic mean (lines in A, C, E, G, I, K, M, and O; horizontal bars in B, D, F, H, J, L, N, and P) ± SEM. The p values were calculated by one-way ANOVA and Holm-Sidak post-test. *p < 0.05, **p < 0.01; atr., atropine; Glc, glucose; ipa-br, ipratropium bromide; darif, darifenacin; AUC, area under the curve.

See also Figure S1.

note, the dose used in these experiments was half the amount used for experiments evaluating the effects of i.p. injection of IL-1Ra in the cephalic phase (Figures 3A and 3B). However, similar to the IL-1β effect described above, IL-1Ra also leaked into the systemic circulation (Figure 4D), even at a 10-fold lower dose (Figure S3A). Therefore, we performed the cephalic phase

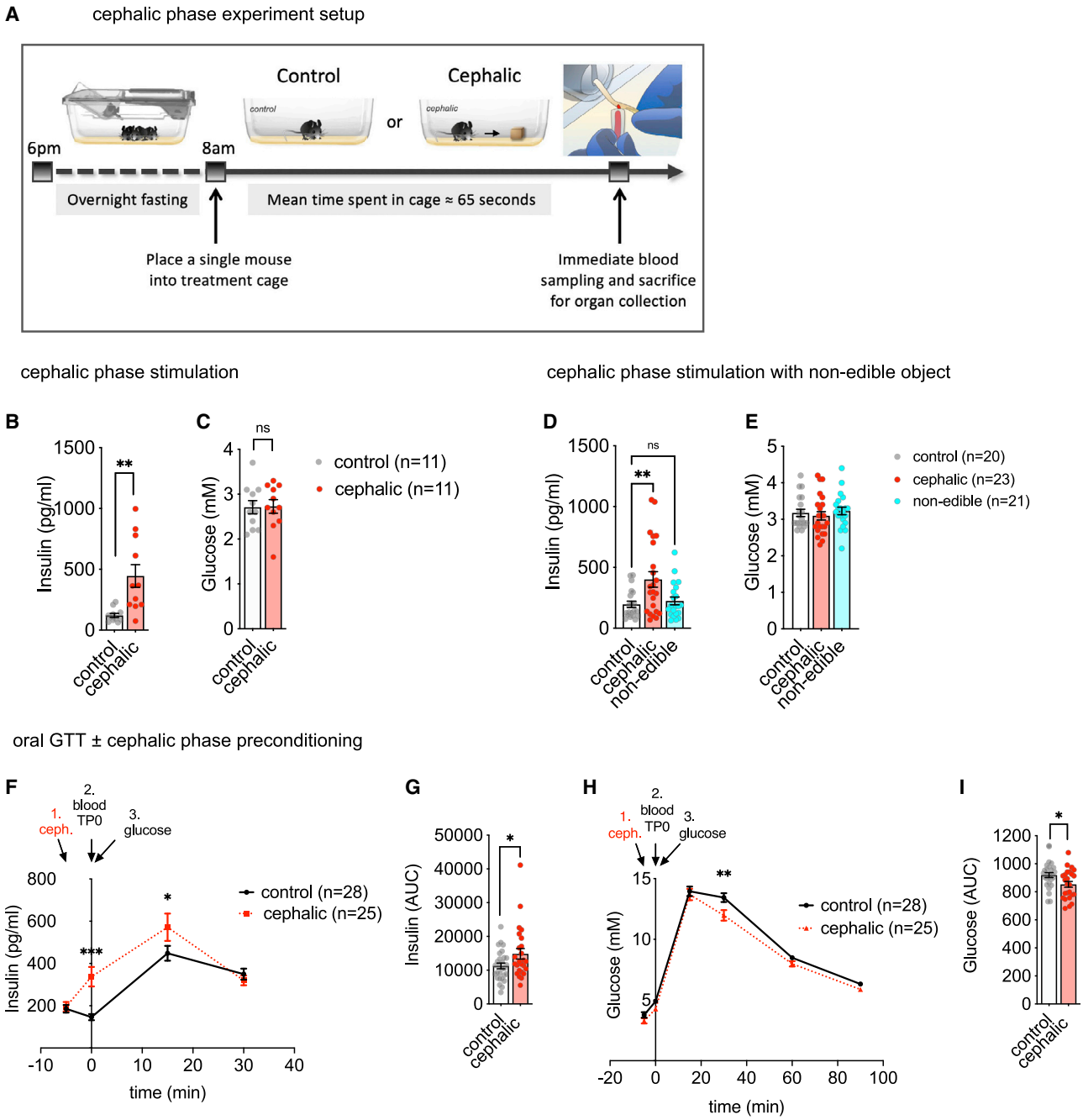

Figure 2. Cephalic phase model

(A) Schematic representation of the cephalic phase experimental model.

(B–I) Animals used in these experiments were female wild-type C57BL/6NCrl mice. The control groups were fasted mice.

(B and C) Measurements after cephalic phase stimulation.

(D and E) Measurement after cephalic phase stimulation with a non-edible object.

(F–I) Measurements during an oral GTT after cephalic phase pre-conditioning. Oral glucose bolus (2 g/kg BW) T = 0 min.

Data are presented as individual measurements (points in B–E, G, and I) and arithmetic mean (lines in F and H; horizontal bars in B–E, G, and I) ± SEM. The p values of (B, C, G, and I) were calculated by Student's unpaired two-sample t test, and the p values of (D and E) were calculated by one-way ANOVA and Holm-Sidak post-test. The p values of graphs (F and H) were calculated over all time points of the comparison of control (fasted) and cephalic stimulated by two-way ANOVA and Holm-Sidak post-test. *p < 0.05, **p < 0.01; ceph., cephalic stimulation; blood TP0, blood sampling at time point 0 min before glucose application; AUC, area under the curve.

See also Video S1 and Figure S2.

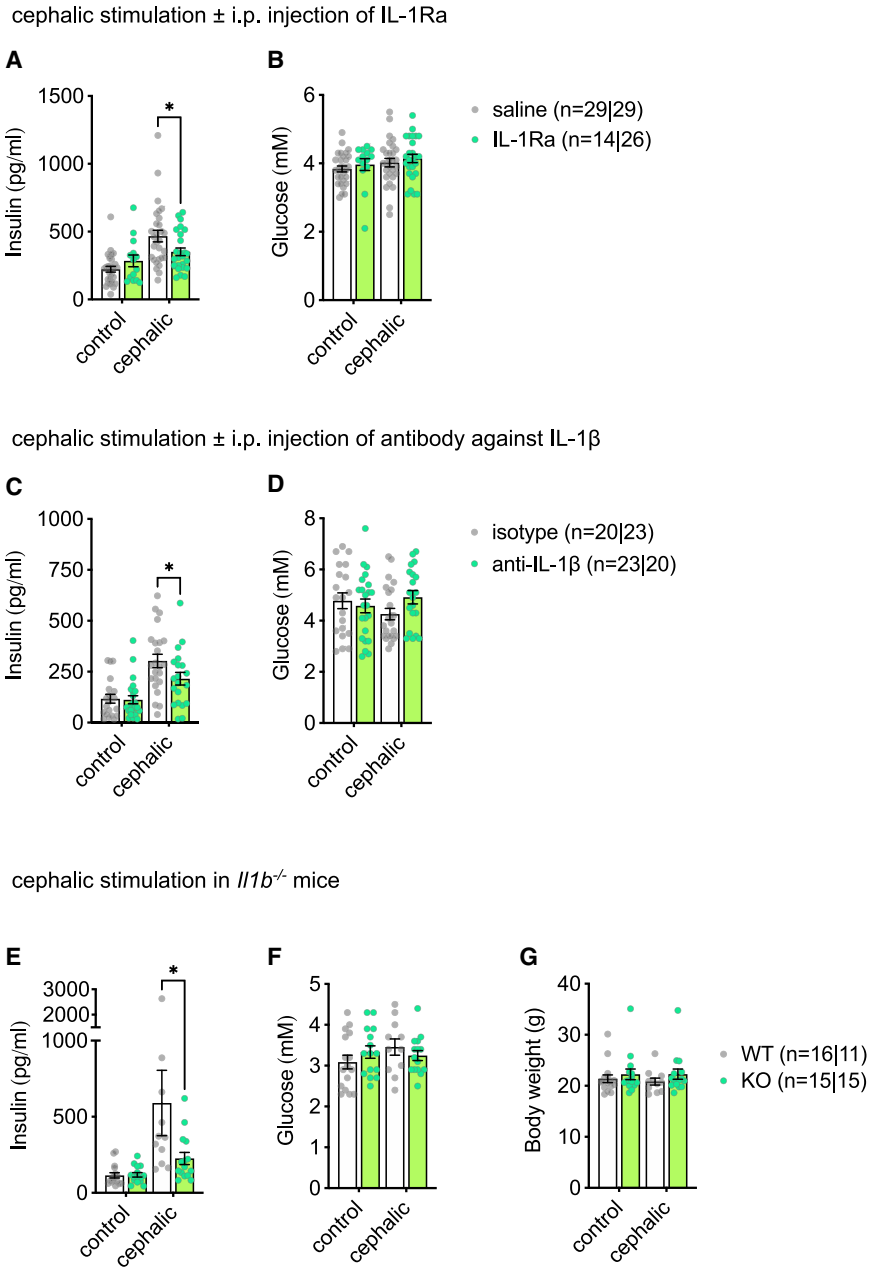

Figure 3. Cephalic phase insulin release is mediated by IL-1β

(A–F) Insulin and glucose concentrations following cephalic phase stimulation. The control groups were fasted mice. For the number of replicates, the format n = (control|cephalic) was used.

(A and B) Measurements of female wild-type C57BL/6NCrl mice i.p. injected with 25 mg/kg BW recombinant human IL-1Ra or saline 1 h and −20 mins prior to cephalic phase stimulation (= two injections total).

(C and D) Measurements of female wild-type C57BL/6NCrl mice i.p. injected with 10 mg/kg BW mouse anti-IL-1β or isotype control 30 min prior to cephalic phase stimulation.

(E–G) Measurements of female wild-type C57BL/6NCrl and littermate Il1b$^{-/-}$ mice.

Data are presented as individual measurements (points) and arithmetic mean (horizontal bars) ± SEM. The p values were calculated by two-way ANOVA and Holm-Sidak post-test. *p < 0.05; WT, wild-type; KO, knockout. The data as shown in graphs (A and E) analyzed with robust nonlinear regression model (ROUT,Q = 1%, GraphPad Prism) to identify and remove outliers (data not shown) still have significant p values; 0.0459 and 0.0221, respectively.

experiments in myeloid cell-specific *Il1b* KO mice (*Lyz2*-Cre *Il1b*$^{fl/fl}$). Interestingly, these mice showed no impairment in cephalic phase insulin secretion compared with littermate controls (Figures 4E, 4F, and S3B), arguing against *Lyz2-expressing* myeloid cells as a cellular source for cephalic phase IL-1β. However, while highly expressed in peripheral tissue macrophages and monocytes (Böni-Schnetzler et al., 2021), the *Lyz2*-Cre promoter shows only about 45% recombination efficiency in microglia (Goldmann et al., 2013). In support of a central source for IL-1β, refeeding of WT mice induced an increase of *Il1b* gene expression in microglia sorted from the whole brain (Figure 4G). Moreover, we localized this increase in *Il1b* gene expression specifically to microglia in the hypothalamus (Figure 4H). To test whether microglia are the source of IL-1β also in the cephalic phase, we used the *Cx3cr1*-Cre^{ERT2}*Tak1*$^{fl/fl}$ (Goldmann et al., 2013) mouse strain. *Cx3cr1* is highly expressed in microglia, although it targets other peripheral macrophages and circulating monocytes as well (Jung et al., 2000). Due to the longevity of microglia (Ajami et al., 2007), the induction of *Cx3cr1*-Cre^{ERT2} with tamoxifen over time restricts the active *Cx3cr1*-Cre^{ERT2} expression to microglia, while other shorter-lived *Cx3cr1*-expressing cells are continuously replaced with Cre-inactive precursor cells (Goldmann et al., 2013). Although this mouse model is highly efficient in targeting microglia and other myeloid cells of the CNS, it also targets long-lived peripheral macrophage subsets like islet macrophages and liver macrophages, but to a lesser extent (Figures S3C, S4A, and S4B for gating strategies). The deletion of *Tak1* impairs central inflammatory signaling nodes like NF-κB and thus leads to the impaired expression of many cytokines, chemokines, and adhesion molecules including IL-1β (Goldmann et al., 2013). We performed the cephalic phase experiments with *Cx3cr1*-Cre^{ERT2} *Tak1*$^{fl/fl}$ mice and their Cre-negative littermate controls. Four weeks post Cre-induction, both male and female *Cx3cr1*-Cre^{ERT2} *Tak1*$^{fl/fl}$ mice showed impaired cephalic phase insulin release (Figures 4I, 4J, and S3D). Additionally, *Cx3cr1*-Cre^{ERT2} *Tak1*$^{fl/fl}$ mice had similar basal IL-1β levels relative to their littermate controls (Figure 4K). Next, to more specifically target IL-1β expression in microglia, we generated *Cx3cr1*-Cre^{ERT2} *Il1b*$^{fl/fl}$ mice. Microglia isolated from *Cx3cr1*-Cre^{ERT2} *Il1b*$^{fl/fl}$ mice had significantly reduced *Il1b* expression compared with

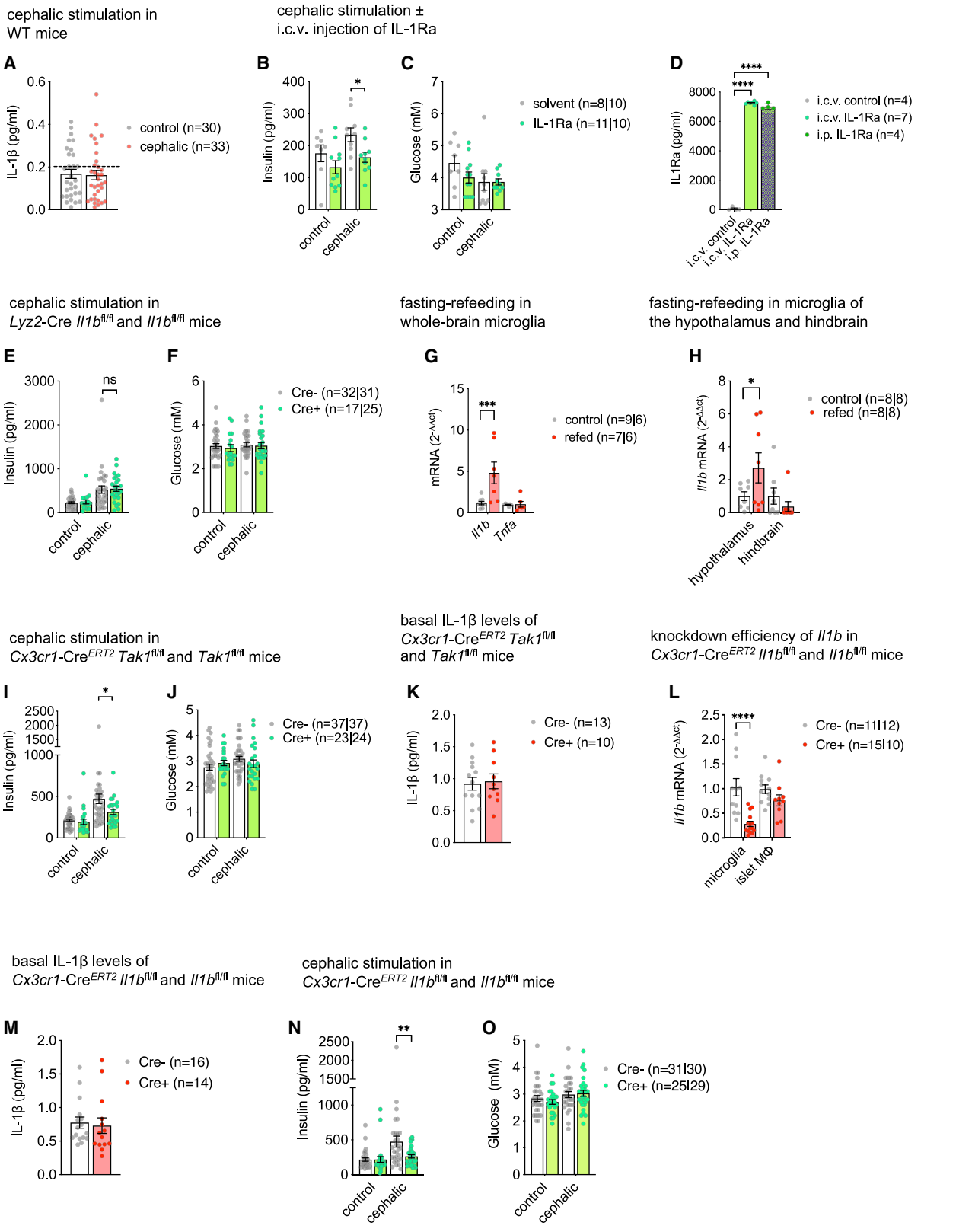

(legend on next page)

long-lived peripheral islet macrophages (Figure 4L). Basal IL-1β levels of *Cx3cr1*-Cre^{ERT2} *Il1b*$^{fl/fl}$ mice were similar to their littermate controls (Figure 4M). *Cx3cr1*-Cre^{ERT2} *Il1b*$^{fl/fl}$ mice were subjected to the cephalic phase experiments eight weeks after Cre-induction, and both male and female mice exhibited impaired insulin secretion (Figures 4N, 4O, and S3E). Importantly, tamoxifen-induced mice expressing only *Cx3cr1*-Cre^{ERT2} did not show altered cephalic phase insulin response when compared with Cre-negative littermate controls (Figures S3F–S3H). In summary, IL-1β originating from long-lived CX3CR1+ myeloid cells controls the cephalic phase of insulin secretion.

IL-1β regulates neuronal activity in the paraventricular nucleus of the hypothalamus in response to cephalic stimulation

To demonstrate the involvement of muscarinic receptor signaling in our cephalic phase model, we treated mice with atropine prior to cephalic stimulation and observed impaired cephalic phase insulin release (Figures 5A and 5B). Next, we found that IL-1β increased basal vagus nerve activity, and this showed strong synergistic effects with glucose (Figure 5C), indicating that IL-1β is capable of increasing vagal output both at low glucose concentrations (as is the case during cephalic stimulation) and in a glucose-dependent manner (as is the case postprandially). Then, we measured neuronal activity within the paraventricular nucleus of the hypothalamus (PVH), the area postrema (AP), the nucleus tractus solitarius (NTS), and the dorsal motor nucleus of the vagus (DMV) via quantification of c-Fos protein expression. Inhibition of IL-1 signaling with IL-1Ra injected i.c.v. increased c-Fos protein expression upon cephalic stimulation specifically within the PVH (Figures 5D and 5E), but not the NTS, AP, or DMV (Figure S5). These data show that IL-1β stimulates vagal nerve activity in a glucose-dependent manner and that IL-1 signaling during the cephalic phase limits neuronal activity in the PVH.

Cephalic phase insulin secretion is impaired in obesity, which may be prevented by the inhibition of IL-1β

Since IL-1β signaling is required for normal cephalic phase insulin secretion, we wondered what influence chronic inflammation, as observed in obesity, would have on this response. First, we performed a pre-specified secondary analysis of our published meta-analysis on cephalic phase insulin release in humans (Wiedemann et al., 2020). This analysis showed that obesity had a significant negative impact on the effect size of cephalic phase insulin release ($F(df1 = 1, df2 = 75) = 5.40$, $p = 0.023$; Figures 6A and 6B). Next, we reproduced these human data in our mouse model and found that cephalic phase insulin release was abolished after only two weeks of high-fat diet (HFD) feeding (Figures 6C and S6A). This impairment of cephalic phase insulin release in obesity was furthermore accompanied by a loss of the positive effect of cephalic-preconditioning on glucose tolerance following a glucose bolus (Figures 6D–6G compared with Figures 2F–2I). Pre-treatment with a mouse anti-IL-1β antibody (1 injection weekly over a period of 3 weeks) prevented the impairment in cephalic phase insulin release upon 3 weeks of HFD feeding (Figures 6H–6L, S6B, and S6C). This indicates that a chronic excess of endogenous IL-1β activity due to obesity dysregulates the cephalic phase of insulin release in humans and mice, and this can be prevented by IL-1β antagonism.

DISCUSSION

We show that IL-1β modulated insulin secretion via stimulation of the parasympathetic nervous system. Accordingly, pharmacological inhibition of parasympathetic nerve transmission inhibited the stimulation of insulin secretion by IL-1β. Indeed, the application of IL-1β increased vagus nerve activity, and this effect was potentiated by glucose. This is reminiscent of the enhancement of glucose-stimulated insulin secretion by IL-1β (Dror et al., 2017). As vagal fibers express the IL-1 receptor (Goehler et al., 1997), IL-1β may prime the vagus nerve for glucose stimulation.

Figure 4. Cephalic phase IL-1β originates from long-lived CX3CR1+ cells

(A) Serum IL-1β concentrations following cephalic stimulation in female wild-type C57BL/6NCrl mice. Sample concentrations below the detection limit of the commercial test (= dotted line) represent extrapolated data points.

(B, C, E–J, N, and O) The control groups were fasted mice. For the number of replicates, the format n = control|cephalic was used.

(B and C) Measurements in female wild-type C57BL/6NCrl mice that received an i.c.v. injection of either 25 mg/kg BW IL-1Ra or solvent 1 h prior to cephalic phase stimulation.

(D) Plasma concentrations of human IL-1Ra in female mice 1 h after i.p. or i.c.v. injection of 25 mg/kg BW recombinant human IL-1Ra or solvent.

(E and F) Measurements after cephalic phase stimulation in female *Lyz2*-Cre *Il1b*$^{fl/fl}$ and their littermate *Il1b*$^{fl/fl}$ mice.

(G) Relative mRNA expression of FACS-sorted whole-brain microglia of male wild-type C57BL/6NCrl mice following fasting-refeeding experiment.

(H) Relative *Il1b* mRNA expression of FACS-sorted microglia from different brain regions of female wild-type C57BL/6NCrl mice following the fasting-refeeding experiment (values were normalized to the control of the corresponding brain region).

(I and J) Measurements after cephalic phase stimulation in male and female *Cx3cr1*-Cre^{ERT2} *Tak1*$^{fl/fl}$ and their littermate *Tak1*$^{fl/fl}$ mice 4 weeks after the induction with tamoxifen.

(K) Fasted serum IL-1β levels of male and female *Cx3cr1*-Cre^{ERT2} *Tak1*$^{fl/fl}$ and their littermate *Tak1*$^{fl/fl}$ mice.

(L) Relative *Il1b* mRNA expression of FACS-sorted microglia and isolated islets from *Cx3cr1*-Cre^{ERT2} *Il1b*$^{fl/fl}$ and their littermate *Il1b*$^{fl/fl}$ mice 8 weeks after the induction with tamoxifen (values were normalized to Cre-negative littermates). For the number of replicates, the format n = microglia|islet macrophage was used.

(M) Fasted serum IL-1β levels of male and female *Cx3cr1*-Cre^{ERT2} *Il1b*$^{fl/fl}$ and their littermate *Il1b*$^{fl/fl}$ mice.

(N and O) Measurements after cephalic phase stimulation in male and female *Cx3cr1*-Cre^{ERT2} *Il1b*$^{fl/fl}$ and their littermate *Il1b*$^{fl/fl}$ mice.

Data are presented as individual measurements and arithmetic mean ± SEM. The p values of (A, K, and M) were calculated by a Student's unpaired two-sample t test. The p values of (D) were calculated by one-way ANOVA and Holm-Sidak post-test. The p values of (B, C, E–J, L, N, and O) were calculated by two-way ANOVA and Holm-Sidak post-test (B, C, E–G, I, J, L, N, and O) or Fisher's LSD test (H). *$p < 0.05$, ***$p < 0.001$; i.c.v., intracerebroventricular injection; i.p., intraperitoneal injection; Mφ, macrophages. The data as shown in graphs (I and N) analyzed with ROUT (Q = 1%, GraphPad Prism) to identify and remove outliers (data not shown) still have significant p values; 0.0226 and 0.0018, respectively.

See also Figures S3 and S4.

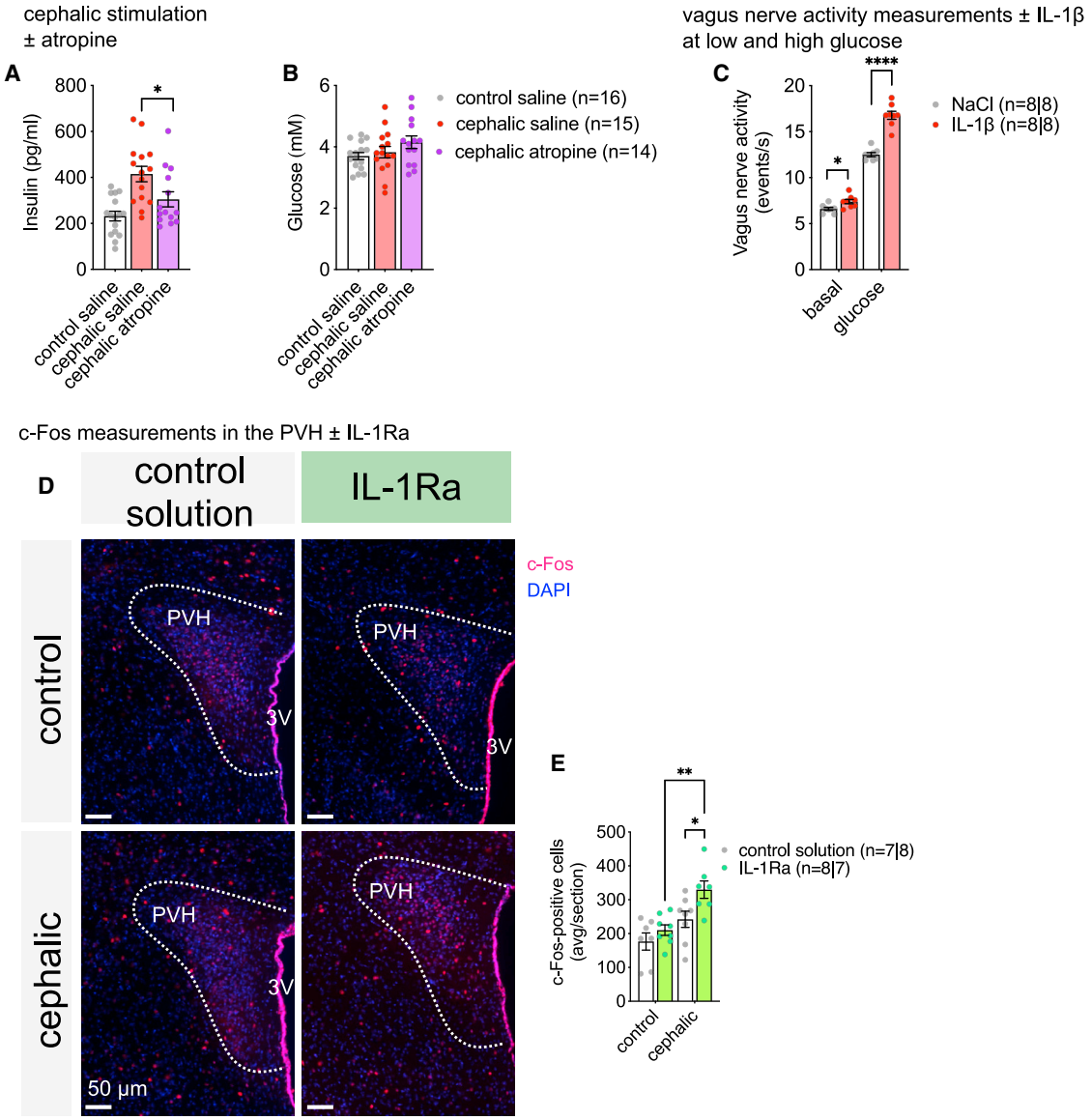

Figure 5. IL-1β modulates neuronal activity in response to cephalic stimulation

(A and B) Measurements after cephalic phase stimulation in male wild-type C57BL/6NCrl mice. Mice were i.p. injected either with atropine (5 mg/kg) or saline at T = −20 min. Control group was fasted mice.

(C) Electrophysical measurements of vagus nerve activity in female wild-type C57BL/6NCrl mice following an i.p. injection of either saline or IL-1β (1 μg/kg BW) at T = −10 min and a second injection of saline or glucose (2 g/kg BW) at T = +5 min.

(D) Representative brain tissue sections stained with DAPI in blue and with anti-c-Fos antibody in red. Female wild-type C57BL/6NCrl mice received one i.c.v. injection of either 25 mg/kg BW IL-1Ra or solvent 1 h prior to cephalic stimulation.

(E) Quantification of c-Fos-positive cells in the PVH (average per histological section).

Data are presented as individual measurements (points in A–C and E) and arithmetic mean (horizontal bars in A–C and E) ± SEM. For the number of replicates in (C) the format (n = low|high) glucose was used. For the number of replicates in (E), the format (n = control|cephalic) was used. The p values were calculated by either Student's unpaired two-sample t test (C) or one-way ANOVA and Holm-Sidak post-test (A). *p < 0.05, **p < 0.01, ****p < 0.001; PVH, paraventricular nucleus of the hypothalamus.

See also Figure S5.

Supporting the role of IL-1β in the neuronal regulation of insulin, we show that cephalic phase insulin release was modulated by IL-1β derived from CX3CR1+ myeloid cells. Furthermore, cephalic phase insulin secretion was impaired in obesity in humans and mice, and this was prevented by chronic inhibition of IL-1β in mice.

The cellular source of IL-1β modulating the cephalic phase of insulin secretion is most likely microglia or other CNS-associated macrophages. Equivalently, feeding increased *Il1b* gene expression specifically in hypothalamic microglia. Moreover, the injection of IL-1Ra directly into the cerebrospinal fluid of WT mice

CellPress
OPEN ACCESS

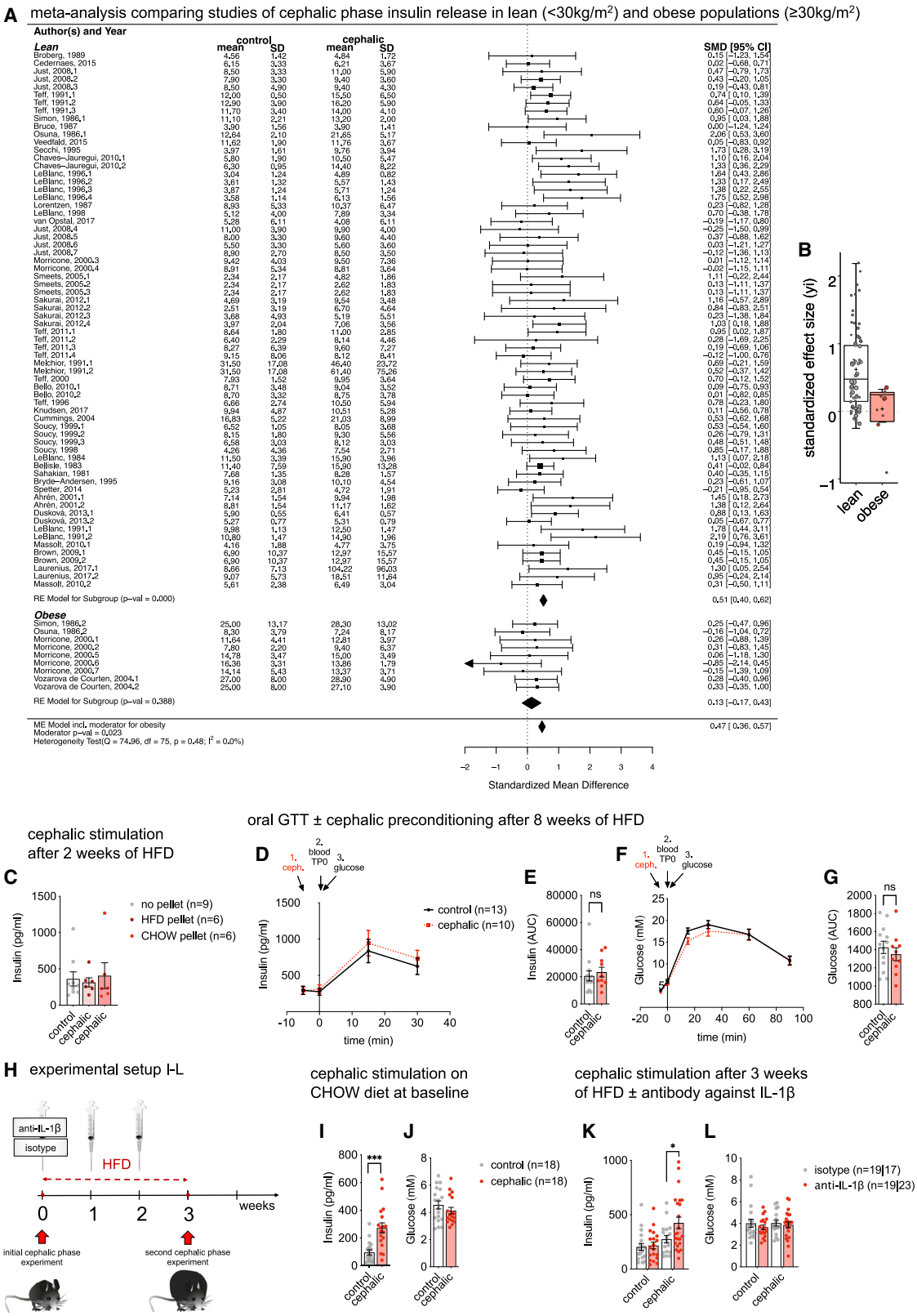

(legend on next page)

reduced cephalic phase insulin release even at half the dose of comparable i.p. injections. However, we saw that i.c.v. injected IL-1Ra and IL-1β leaked into the systemic circulation, and therefore, the central effects might be partly diluted by peripheral effects of IL-1. Arguing against such peripheral IL-1β effects upon i.c.v. injection are the unchanged circulating insulin levels after treatment with a 10-fold lower dose of IL-1β given i.p. and the lack of a rise in systemic IL-1β levels upon cephalic stimulation. This suggests that the source of IL-1β in the cephalic phase is in close contact with its neuronal target cells. Further supporting a central role of IL-1β in cephalic phase insulin secretion is the fact that i.c.v. injected IL-1β stimulated peripheral insulin secretion before escaping to the systemic circulation. Cephalic stimulation was absent when IL-1β was ablated in *Cx3cr1*- but not *Lyz2*-expressing cells. While the *Lyz2*-Cre model only targets about 45% of microglia (Goldmann et al., 2013), we saw a robust knockdown of IL-1β expression (75%) in the microglia of *Cx3cr1-Cre*^{ERT2} *Il1b*$^{fl/fl}$ mice. Additionally, only 16% of islet macrophages expressed yellow fluorescent protein (YFP) in *Cx3cr1*-Cre reporter mice, and YFP expression in immune cells isolated from all other tissues was negligible. These data strongly suggest that microglia are the source of IL-1β relevant for cephalic phase insulin secretion.

Interestingly, central but not peripheral muscarinic blockade reduced the IL-1β stimulatory effect on insulin secretion. This suggests that muscarinic receptors expressed on pancreatic islets are not involved in the stimulatory effects of IL-1β on insulin secretion.

Since cephalic phase insulin release is a rapid physiological response to food stimuli, reaching its peak already 2–3 min after food exposure (Berthoud et al., 1980), it would require quick signaling cascades. We hypothesize that microglia promptly release preformed vesicles of IL-1β upon cephalic stimulation as it has been described in response to environmental signals such as ATP (Fassbender et al., 2000; Monif et al., 2016). Indeed, a similar rapid response to sensory food stimulus has been observed in the agouti-related peptide neurons of the arcuate nucleus (Chen et al., 2015). Alternatively, IL-1β may act as a tonic signal in which a certain level of IL-1β is required for proper signaling of the cephalic phase neuronal circuitry.

Previous reports on disturbed cephalic phase insulin response in obese human individuals are conflicting (Johnson and Wildman, 1983; Lieverse et al., 1994; Morricone et al., 2000; Osuna et al., 1986; Parra-Covarrubias et al., 1971; Rodin, 1978; Simon et al., 1986; Sjöström et al., 1980; Teff et al., 1993). Teff et al. suggested that these differing observations might be reconciled by the fact that obese individuals show higher baseline insulin values than controls, and our data support this line of argumentation. Baseline insulin values from the studies assessing obese individuals included in our meta-analysis were twice as high as in the lean group (mean ± 95% CI—lean: 8.07 ± 1.23 mIU/L, obese: 16.67 ± 5.63 mIU/L), and we saw a significant reduction in cephalic phase insulin release effect size when comparing studies assessing lean with studies assessing obese populations. Of note, standardized mean differences already correct for both the baseline and variance of a study by design (Deeks et al., 2019).

Our mouse experiments further support this line of reasoning. Cephalic phase insulin release in mice was impaired after 2 weeks of HFD feeding. This was characterized by basal hyperinsulinemia and failure to further increase insulin secretion upon cephalic stimulation. In light of the chronic low-grade inflammation present in obesity (Carstensen et al., 2010; Herder and Brunner, 2009; Larsen et al., 2007; Meier et al., 2002; Spranger et al., 2003), this may reflect a chronic neuronal stimulation of insulin. Congruently, obesity is associated with hypothalamic inflammation characterized by the accumulation of microglia and the expression of proinflammatory cytokines including IL-1β (De Souza et al., 2005; Milanski et al., 2009; Thaler et al., 2012). Accordingly, anti-IL-1β-therapy enabled HFD-fed mice to further increase insulin release upon cephalic stimulation. Therefore, our data support the notion that the impairment of cephalic phase responses upon HFD feeding is an IL-1β-dependent mechanism and indicate a causal role for IL-1β in the dysregulation of autonomic neuronal responses in obesity.

In summary, our findings attribute a regulatory role to IL-1β in the integration of nutrient-derived sensory information, subsequent neuronally mediated insulin secretion, and the dysregulation of autonomic cephalic phase responses in obesity. This identifies a neuro-immunologic endocrine circuit in the regulation of insulin secretion.

Figure 6. Cephalic phase insulin secretion is impaired in obesity, which may be prevented by the inhibition of IL-1β

(A) Forest plot of the meta-analysis assessing studies of cephalic phase inulin release with "lean" versus "obese" trial populations. The mean and standard deviation of control and cephalic insulin values (mIU/L) for each trial population are listed.

(B) Boxplot of standardized effect size estimates for the groups described in (A). The point size increases with sampling variance.

(C) Circulating insulin concentration following cephalic stimulation in female wild-type C57BL/6NCrl mice after 2 weeks of HFD feeding. For cephalic stimulation, mice were either presented with a regular CHOW or HFD pellet.

(D–G) Measurements after cephalic stimulation in female wild-type C57BL/6NCrl mice fed HFD for 8 weeks and then cephalic stimulated (or not) prior to an oral glucose bolus (2 g/kg BW).

(H) Schematic representation of HFD feeding with mouse anti-IL-1β treatment.

(I and J) Measurements after cephalic stimulation in female wild-type C57BL/6NCrl before HFD feeding.

(K and L) Measurements after cephalic stimulation in female wild-type C57BL/6NCrl after 3 weeks of HFD feeding and mouse anti-IL-1β treatment or isotype control. For the number of replicates, the format n = control|cephalic was used.

Data are presented as individual measurements (points in C, E, G, and I–L), overall arithmetic mean (lines in D and F, horizontal bars in C, E, G, and I–L) ± SEM. p values were calculated by Student's unpaired two-sample t test in (E), (G), (I), and (J). p values of (C) were calculated by one-way ANOVA and Holm-Sidak post-test. p values for (K) and (L) were calculated by two-way ANOVA and Holm-Sidak post-test. *$p < 0.05$, ***$p < 0.001$; AUC, area under the curve; HFD, high-fat diet; ceph., cephalic phase stimulation; blood TP0, blood sampling at time point 0 min before glucose gavage; SD, standard deviation, SMD, standardized mean difference; CI, confidence interval; RE, random-effects; p val, p value; Q, Cochrane Q; df, degrees of freedom; p, p value; I^2, Higgins and Thomsons' I.

See also Figure S6.

Limitations of the study

We demonstrated that IL-1β induces insulin secretion via the stimulation of parasympathetic nerves. However, it is likely that additional pathways are involved, since the insulin-stimulating effect of IL-1β was only partially blocked by muscarinic inhibition. It is conceivable that IL-1β may also exert direct effects on β cells (Böni-Schnetzler and Meier, 2019). Furthermore, although we were able to narrow down the source of IL-1β to CX3CR1+ cells of the CNS, the precise mechanisms coupling IL-1β to rapid neuronal activation remain to be explored. In this context, the observed changes in c-Fos expression levels during cephalic stimulation in various regions of the hypothalamus do not allow precise mapping of the neurons involved in the signaling cascade leading to insulin secretion.

STAR★METHODS

Detailed methods are provided in the online version of this paper and include the following:

- KEY RESOURCES TABLE
- RESOURCE AVAILABILITY
  - Lead contact
  - Materials availability
  - Data and code availability
- EXPERIMENTAL MODEL AND SUBJECT DETAILS
  - Animals
- METHOD DETAILS
  - Cephalic phase experiments
  - Glucose tolerance tests
  - Fasting-refeeding experiments
  - High-fat diet feeding experiments
  - Basal IL-1beta protein measurements
  - Intracerebroventricular cannula implantation
  - Vagus nerve activity measurements
  - Histology and c-FOS quantification
  - Primary cell isolation
  - RNA-extraction and qPCR
  - Flow cytometry
  - Protein measurement assays
- QUANTIFICATION AND STATISTICAL ANALYSIS
  - General information
  - Meta-analysis
- ADDITIONAL RESOURCES

SUPPLEMENTAL INFORMATION

Supplemental information can be found online at https://doi.org/10.1016/j.cmet.2022.06.001.

ACKNOWLEDGMENTS

This study was funded by the Margot und Erich Goldschmidt & Peter René Jacobson-Stiftung (S.J.W.), the alumni of the medical faculty of the University of Basel (S.J.W.), and the Swiss National Research Foundation. Funding entities had no role in the study design, data collection, data analysis, data interpretation, writing of the paper, or decision to submit the paper for publication. We thank Alexandre Picard for his help in establishing the implantation of intracerebroventricular cannulas in our lab and the Hutter Group of the Department of Biomedicine of the University Hospital of Basel for letting us borrow their stereotactic frame and neurosurgical drill for the implantations. We also thank Emmanuel Traunecker, Lorenzo Raeli, Danny Labes, and Telma Lopes for help sorting immune cell subsets and Ueli Schneider, Nicole Caviezel, Dominik Viscardi, and the rest of the team of the animal facility at the University Hospital Basel for taking excellent care of our laboratory animals. We also thank Sebastian Olschewski for advice regarding statistical analyses.

AUTHOR CONTRIBUTIONS

E.D. conceptualized the cephalic phase mouse model. S.J.W., K.T., E.D., M.B.-S., and M.Y.D. designed the experiments. C.M. performed the vagus nerve activity measurements. C.L.F. performed c-Fos stainings. S.J.W., K.T., and E.D. performed all the other experiments. J.A.M.-T., L.R., D.T.M., F.S., M.S., S.P.H., and H.M. helped with experiments conducted in Basel. S.J.W. and K.T. performed the statistical analysis. S.J.W., K.T., M.B.-S., D.T.M., and M.Y.D. wrote the manuscript. All authors interpreted the data, revised the paper critically for important intellectual content, approved the final version of the manuscript, and agreed to be responsible for all aspects of the work.

DECLARATION OF INTERESTS

M.Y.D. is listed as the inventor on a patent filed in 2003 for the use of an IL-1 receptor antagonist for the treatment of or prophylaxis for type 2 diabetes.

Received: March 16, 2021
Revised: February 1, 2022
Accepted: June 1, 2022
Published: June 23, 2022

REFERENCES

Ahrén, B. (2000). Autonomic regulation of islet hormone secretion – implications for health and disease. Diabetologia *43*, 393–410.

Ahrén, B., Karlsson, S., and Lindskog, S. (1990). Cholinergic regulation of the endocrine pancreas. In Progress in Brain Research, Chapter 23, S.-M. Aquilonius and P.-G. Gillberg, eds. (Elsevier), pp. 209–218.

Ajami, B., Bennett, J.L., Krieger, C., Tetzlaff, W., and Rossi, F.M. (2007). Local self-renewal can sustain CNS microglia maintenance and function throughout adult life. Nat. Neurosci. *10*, 1538–1543.

Andersen, H.B., Christiansen, E., Vølund, A., Madsbad, S., Rasmussen, K., Burcharth, F., and Christensen, N.J. (1995). Sham feeding increases glucose tolerance by a mechanism independent of insulin secretion in normal subjects. Digestion *56*, 253–258.

Bendtzen, K., Mandrup-Poulsen, T., Nerup, J., Nielsen, J.H., Dinarello, C.A., and Svenson, M. (1986). Cytotoxicity of human pI 7 interleukin-1 for pancreatic islets of Langerhans. Science *232*, 1545–1547.

Berthoud, H.R. (1984). The relative contribution of the nervous system, hormones, and metabolites to the total insulin response during a meal in the rat. Metabolism *33*, 18–25.

Berthoud, H.R., Bereiter, D.A., Trimble, E.R., Siegel, E.G., and Jeanrenaud, B. (1981). Cephalic phase, reflex insulin secretion. Neuroanatomical and physiological characterization. Diabetologia *20* (*Suppl 1*), 393–401.

Berthoud, H.R., and Jeanrenaud, B. (1982). Sham feeding-induced cephalic phase insulin release in the rat. Am. J. Physiol. *242*, E280–E285.

Berthoud, H.R., Trimble, E.R., Siegel, E.G., Bereiter, D.A., and Jeanrenaud, B. (1980). Cephalic-phase insulin secretion in normal and pancreatic islet-transplanted rats. Am. J. Physiol. *238*, E336–E340.

Böni-Schnetzler, M., and Meier, D.T. (2019). Islet inflammation in type 2 diabetes. Semin. Immunopathol. *41*, 501–513.

Böni-Schnetzler, M., Méreau, H., Rachid, L., Wiedemann, S.J., Schulze, F., Trimigliozzi, K., Meier, D.T., and Donath, M.Y. (2021). IL-1beta promotes the age-associated decline of beta cell function. iScience *24*, 103250.

Böni-Schnetzler, M., Thorne, J., Parnaud, G., Marselli, L., Ehses, J.A., Kerr-Conte, J., Pattou, F., Halban, P.A., Weir, G.C., and Donath, M.Y. (2008). Increased interleukin (IL)-1beta messenger ribonucleic acid expression in β-cells of individuals with type 2 diabetes and regulation of IL-1β in human

islets by glucose and autostimulation. J. Clin. Endocrinol. Metab. *93*, 4065–4074.

Brede, S., Lutzke, B., Albers, E., Dalla-Man, C., Cobelli, C., Hallschmid, M., Klement, J., and Lehnert, H. (2020). Visual food cues decrease blood glucose and glucoregulatory hormones following an oral glucose tolerance test in normal-weight and obese men. Physiol. Behav. *226*, 113071.

Brede, S., Sputh, A., Hartmann, A.-C., Hallschmid, M., Lehnert, H., and Klement, J. (2017). Visual food cues decrease postprandial glucose concentrations in lean and obese men without affecting food intake and related endocrine parameters. Appetite *117*, 255–262.

Brykczynska, U., Geigges, M., Wiedemann, S.J., Dror, E., Böni-Schnetzler, M., Hess, C., Donath, M.Y., and Paro, R. (2020). Distinct transcriptional responses across tissue-resident macrophages to short-term and long-term metabolic challenge. Cell Rep. *30*, 1627–1643.e7.

Carstensen, M., Herder, C., Kivimäki, M., Jokela, M., Roden, M., Shipley, M.J., Witte, D.R., Brunner, E.J., and Tabák, A.G. (2010). Accelerated increase in serum interleukin-1 receptor antagonist starts 6 years before diagnosis of type 2 diabetes: Whitehall II prospective cohort study. Diabetes *59*, 1222–1227.

Casarosa, P., Bouyssou, T., Germeyer, S., Schnapp, A., Gantner, F., and Pieper, M. (2009). Preclinical evaluation of long-acting muscarinic antagonists: comparison of tiotropium and investigational drugs. J. Pharmacol. Exp. Ther. *330*, 660–668.

Chen, Y., Lin, Y.C., Kuo, T.W., and Knight, Z.A. (2015). Sensory detection of food rapidly modulates arcuate feeding circuits. Cell *160*, 829–841.

Coester, B., Pence, S.W., Arrigoni, S., Boyle, C.N., Le Foll, C., and Lutz, T.A. (2020). RAMP1 and RAMP3 differentially control amylin's effects on food intake, glucose and energy balance in male and female mice. Neuroscience *447*, 74–93.

Dalmas, E., Lehmann, F.M., Dror, E., Wueest, S., Thienel, C., Borsigova, M., Stawiski, M., Traunecker, E., Lucchini, F.C., Dapito, D.H., et al. (2017). Interleukin-33-activated islet-resident innate lymphoid cells promote insulin secretion through myeloid cell retinoic acid production. Immunity *47*, 928–942.e7.

De Souza, C.T., Araujo, E.P., Bordin, S., Ashimine, R., Zollner, R.L., Boschero, A.C., Saad, M.J., and Velloso, L.A. (2005). Consumption of a fat-rich diet activates a proinflammatory response and induces insulin resistance in the hypothalamus. Endocrinology *146*, 4192–4199.

Deeks, J.J., Higgins, J.P.T., and Altman, D.G. (2019). Analysing data and undertaking meta-analyses. In Cochrane Handbook for Systematic Reviews of Interventions (John Wiley & Sons), pp. 241–284.

Dinarello, C.A. (2013). Overview of the interleukin-1 family of ligands and receptors. Semin. Immunol. *25*, 389–393.

Donath, M.Y., Dinarello, C.A., and Mandrup-Poulsen, T. (2019). Targeting innate immune mediators in type 1 and type 2 diabetes. Nat. Rev. Immunol. *19*, 734–746.

Donath, M.Y., and Shoelson, S.E. (2011). Type 2 diabetes as an inflammatory disease. Nat. Rev. Immunol. *11*, 98–107.

Dror, E., Dalmas, E., Meier, D.T., Wueest, S., Thévenet, J., Thienel, C., Timper, K., Nordmann, T.M., Traub, S., Schulze, F., et al. (2017). Postprandial macrophage-derived IL-1β stimulates insulin, and both synergistically promote glucose disposal and inflammation. Nat. Immunol. *18*, 283–292.

Duttaroy, A., Zimliki, C.L., Gautam, D., Cui, Y., Mears, D., and Wess, J. (2004). Muscarinic stimulation of pancreatic insulin and glucagon release is abolished in M_3 muscarinic acetylcholine receptor–deficient mice. Diabetes *53*, 1714–1720.

Fassbender, K., Schneider, S., Bertsch, T., Schlueter, D., Fatar, M., Ragoschke, A., Kühl, S., Kischka, U., and Hennerici, M. (2000). Temporal profile of release of interleukin-1beta in neurotrauma. Neurosci. Lett. *284*, 135–138.

Franklin, K.B., and Paxinos, G. (2019). Paxinos and Franklin's the Mouse Brain in Stereotaxic Coordinates, Compact: The Coronal Plates and Diagrams (Academic Press).

Gautam, D., Han, S.-J., Hamdan, F.F., Jeon, J., Li, B., Li, J.H., Cui, Y., Mears, D., Lu, H., Deng, C., et al. (2006). A critical role for β cell M3 muscarinic acetylcholine receptors in regulating insulin release and blood glucose homeostasis in vivo. Cell Metab. *3*, 449–461.

Goehler, L.E., Relton, J.K., Dripps, D., Kiechle, R., Tartaglia, N., Maier, S.F., and Watkins, L.R. (1997). Vagal paraganglia bind bioatinylated interleukin-1 receptor antagonist: a possible mechanism for immune-to-brain communication. Brain Research Bulletin *43*, 357–364.

Goldmann, T., Wieghofer, P., Müller, P.F., Wolf, Y., Varol, D., Yona, S., Brendecke, S.M., Kierdorf, K., Staszewski, O., Datta, M., et al. (2013). A new type of microglia gene targeting shows TAK1 to be pivotal in CNS autoimmune inflammation. Nat. Neurosci. *16*, 1618–1626.

Hajmrle, C., Smith, N., Spigelman, A.F., Dai, X., Senior, L., Bautista, A., Ferdaoussi, M., and MacDonald, P.E. (2016). Interleukin-1 signaling contributes to acute islet compensation. JCI Insight *1*, e86055.

Herder, C., Brunner, E.J., Rathmann, W., Strassburger, K., Tabák, A.G., Schloot, N.C., and Witte, D.R. (2009). Elevated levels of the anti-inflammatory interleukin-1 receptor antagonist precede the onset of type 2 diabetes: the Whitehall II study. Diabetes Care *32*, 421–423.

Holmes, L.J., Storlien, L.H., and Smythe, G.A. (1989). Hypothalamic monoamines associated with the cephalic phase insulin response. Am. J. Physiol. *256*, E236–E241.

Johnson, W.G., and Wildman, H.E. (1983). Influence of external and covert food stimuli on insulin secretion in obese and normal persons. Behav. Neurosci. *97*, 1025–1028.

Jung, S., Aliberti, J., Graemmel, P., Sunshine, M.J., Kreutzberg, G.W., Sher, A., and Littman, D.R. (2000). Analysis of fractalkine receptor CX_3CR1 function by targeted deletion and green fluorescent protein reporter gene insertion. Mol. Cell. Biol. *20*, 4106–4114.

Larsen, C.M., Faulenbach, M., Vaag, A., Vølund, A., Ehses, J.A., Seifert, B., Mandrup-Poulsen, T., and Donath, M.Y. (2007). Interleukin-1-receptor antagonist in type 2 diabetes mellitus. N. Engl. J. Med. *356*, 1517–1526.

Lieverse, R.J., Masclee, A.A., Jansen, J.B., and Lamers, C.B. (1994). Plasma cholecystokinin and pancreatic polypeptide secretion in response to bombesin, meal ingestion and modified sham feeding in lean and obese persons. Int. J. Obes. Relat. Metab. Disord. *18*, 123–127.

Lorentzen, M., Madsbad, S., Kehlet, H., and Tronier, B. (1987). Effect of sham-feeding on glucose tolerance and insulin secretion. Acta endocrinol. *115*, 84–86.

Louis-Sylvestre, J. (1976). Preabsorptive insulin release and hypoglycemia in rats. Am. J. Physiol. *230*, 56–60.

Maedler, K., Sergeev, P., Ris, F., Oberholzer, J., Joller-Jemelka, H.I., Spinas, G.A., Kaiser, N., Halban, P.A., and Donath, M.Y. (2002). Glucose-induced beta cell production of IL-1beta contributes to glucotoxicity in human pancreatic islets. J. Clin. Invest. *110*, 851–860.

Magnan, C., Collins, S., Berthault, M.F., Kassis, N., Vincent, M., Gilbert, M., Pénicaud, L., Ktorza, A., and Assimacopoulos-Jeannet, F. (1999). Lipid infusion lowers sympathetic nervous activity and leads to increased beta-cell responsiveness to glucose. J. Clin. Invest. *103*, 413–419.

Meier, C.A., Bobbioni, E., Gabay, C., Assimacopoulos-Jeannet, F., Golay, A., and Dayer, J.M. (2002). IL-1 receptor antagonist serum levels are increased in human obesity: a possible link to the resistance to leptin? J. Clin. Endocrinol. Metab. *87*, 1184–1188.

Milanski, M., Degasperi, G., Coope, A., Morari, J., Denis, R., Cintra, D.E., Tsukumo, D.M., Anhe, G., Amaral, M.E., Takahashi, H.K., et al. (2009). Saturated fatty acids produce an inflammatory response predominantly through the activation of TLR4 signaling in hypothalamus: implications for the pathogenesis of obesity. J. Neurosci. *29*, 359–370.

Monif, M., Reid, C.A., Powell, K.L., Drummond, K.J., O'Brien, T.J., and Williams, D.A. (2016). Interleukin-1β has trophic effects in microglia and its release is mediated by P2X7R pore. J. Neuroinflammation *13*, 173.

Morricone, L., Bombonato, M., Cattaneo, A.G., Enrini, R., Lugari, R., Zandomenighi, R., and Caviezel, F. (2000). Food-related sensory stimuli are

able to promote pancreatic polypeptide elevation without evident cephalic phase insulin secretion in human obesity. Horm. Metab. Res. *32*, 240–245.

Nauck, M., Stöckmann, F., Ebert, R., and Creutzfeldt, W. (1986). Reduced incretin effect in type 2 (non-insulin-dependent) diabetes. Diabetologia *29*, 46–52.

Osuna, J.I., Pages, I., Motiño, M.A., Rodriguez, E., and Osorio, C. (1986). Cephalic phase of insulin secretion in obese women. Horm. Metab. Res. *18*, 473–475.

Parra-Covarrubias, A., Rivera-Rodriguez, I., and Almaraz-Ugalde, A. (1971). Cephalic phase of insulin secretion in obese adolescents. Diabetes *20*, 800–802.

Paxinos, G., and Franklin, K. (2012). Paxinos and Franklin's the Mouse Brain in Stereotaxic Coordinates, Fourth Edition (Academic Press).

Powley, T.L. (1977). The ventromedial hypothalamic syndrome, satiety, and a cephalic phase hypothesis. Psychol. Rev. *84*, 89–126.

Röder, P.V., Wu, B., Liu, Y., and Han, W. (2016). Pancreatic regulation of glucose homeostasis. Exp. Mol. Med. *48*, e219.

Rodin, J. (1978). Recent Advances in Obesity Research (Newman).

Sharpey-Schäfer, E.A. (1924). The Endocrine Organs: An Introduction to the Study of Internal Secretion (Longmans, Green and Company).

Simon, C., Schlienger, J.L., Sapin, R., and Imler, M. (1986). Cephalic phase insulin secretion in relation to food presentation in normal and overweight subjects. Physiol. Behav. *36*, 465–469.

Sjöström, L., Garellick, G., Krotkiewski, M., and Luyckx, A. (1980). Peripheral insulin in response to the sight and smell of food. Metabolism *29*, 901–909.

Spranger, J., Kroke, A., Möhlig, M., Hoffmann, K., Bergmann, M.M., Ristow, M., Boeing, H., and Pfeiffer, A.F. (2003). Inflammatory cytokines and the risk to develop type 2 diabetes: results of the prospective population-based European Prospective Investigation into Cancer and Nutrition (EPIC)-Potsdam Study. Diabetes *52*, 812–817.

Srinivas, S., Watanabe, T., Lin, C.S., William, C.M., Tanabe, Y., Jessell, T.M., and Costantini, F. (2001). Cre reporter strains produced by targeted insertion of EYFP and ECFP into the ROSA26 locus. BMC Dev. Biol. *1*, 4.

Steffens, A.B. (1976). Influence of the oral cavity on insulin release in the rat. Am. J. Physiol. *230*, 1411–1415.

Strubbe, J.H. (1992). Parasympathetic involvement in rapid meal-associated conditioned insulin secretion in the rat. Am. J. Physiol. *263*, R615–R618.

Strubbe, J.H., Prins, A.J., Bruggink, J., and Steffens, A.B. (1987). Daily variation of food-induced changes in blood glucose and insulin in the rat and the control by the suprachiasmatic nucleus and the vagus nerve. J. Auton. Nerv. Syst. *20*, 113–119.

Teff, K.L., and Engelman, K. (1996). Oral sensory stimulation improves glucose tolerance in humans: effects on insulin, C-peptide, and glucagon. Am. J. Physiol. *270*, R1371–R1379.

Teff, K.L., Mattes, R.D., Engelman, K., and Mattern, J. (1993). Cephalic-phase insulin in obese and normal-weight men: relation to postprandial insulin. Metabolism *42*, 1600–1608.

Thaler, J.P., Yi, C.X., Schur, E.A., Guyenet, S.J., Hwang, B.H., Dietrich, M.O., Zhao, X., Sarruf, D.A., Izgur, V., Maravilla, K.R., et al. (2012). Obesity is associated with hypothalamic injury in rodents and humans. J. Clin. Invest. *122*, 153–162.

Virtanen, R., Kanto, J., Iisalo, E., Iisalo, E.U.M., Salo, M., and Sjövall, S. (1982). Pharmacokinetic studies on atropine with special reference to age. Acta Anaesthesiol. Scand. *26*, 297–300.

Wiedemann, S.J., Rachid, L., Illigens, B., Böni-Schnetzler, M., and Donath, M.Y. (2020). Evidence for cephalic phase insulin release in humans: a systematic review and meta-analysis. Appetite *155*, 104792.

Zinner, N. (2007). Darifenacin: a muscarinic M3-selective receptor antagonist for the treatment of overactive bladder. Expert Opin. Pharmacother. *8*, 511–523.

STAR★METHODS

KEY RESOURCES TABLE

REAGENT or RESOURCE	SOURCE	IDENTIFIER
Antibodies		
anti-mouse CD16/CD32 [clone 93]	Thermo Fisher Scientific	Cat#14-0161-85; RRID: AB_467134
APC anti-mouse CD45 [clone 30-F11]	Thermo Fisher Scientific	Cat#17-0451-83; RRID: AB_469392
PE anti-mouse CD11b [clone M1/70]	Thermo Fisher Scientific	Cat#12-0112-81; RRID: AB_465546
APC anti-mouse CD115 [clone AFS98]	Thermo Fisher Scientific	Cat#17-1152-82; RRID:AB_1210789
PerCP-Cyanine5.5 anti-mouse Ly6C [clone HK1.4]	Thermo Fisher Scientific	Cat#45-5932-82; RRID:AB_2723343
APC-Cy7 anti-mouse Ly6G [clone 1A8]	BioLegend	Cat#127624; RRID:AB_10640819
PE-Cy5 anti-mouse MHC-II [clone M5/114.15.2]	BioLegend	Cat#107612; RRID:AB_313327
APC-Fire750 anti-mouse Ly6G [clone 1A8]	BioLegend	Cat#127651; RRID:AB_2616732
Super Bright 600 anti-mouse CD45 [clone 30-F11]	Thermo Fisher Scientific	Cat#63-0451-82; RRID:AB_2637149
APC anti-mouse P2RY12 [clone S16007D]	BioLegend	Cat#848006; RRID:AB_2721469
PE anti-mouse CD206 [clone MR6F3]	Thermo Fisher Scientific	Cat#12-2061-82; RRID:AB_2637422
PE-Texas Red anti-mouse CD11b [clone M1/70.15]	Thermo Fisher Scientific	Cat#RM2817; RRID:AB_10373548
APC-Cy7 anti-mouse CD3e [clone 145-2C11]	BioLegend	Cat#100330; RRID:AB_1877170
PE-Cy7 anti-mouse B220 [clone RA3-682]	Thermo Fisher Scientific	Cat#25-0452-82; RRID:AB_469627
PE anti-mouse CD4 [clone GK1.5]	Thermo Fisher Scientific	Cat#12-0041-81; RRID:AB_465505
APC anti-mouse CD8a [clone 53-6.7]	Thermo Fisher Scientific	Cat#17-0081-81; RRID:AB_469334
c-Fos (9F6) Rabbit mouse antibody	Cell Signaling Technology	Cat#2250; RRID:AB_2247211
Alexa Fluor® 488 AffiniPure Goat Anti-Rabbit IgG (H+L)	Jackson Immuno Research Labs	Cat#111-545-144; RRID:AB_2338052
Cy™3 AffiniPure Goat Anti-Rabbit IgG (H+L)	Jackson Immuno Research Labs	Cat#111-165-144; RRID:AB_2338006
Chemicals, peptides, and recombinant proteins		
Trypsin	GIBCO	Cat#154000-054
LPS-SM Ultrapure, Purified lipopolysaccharide from Salmonella minnesota R595 - TLR4 ligand	InvivoGen	Cat#tlrl-smlps
Collagenase type 4	Worthington	Cat#CLS-4
DNA-binding dye DAPI	BioLegend	Cat#422801
0.5% Trypsin-EDTA (x10)	Thermo Fisher Scientific	Cat#15400054
Bovine Serum Albumin (Fatty acid free – Low endotoxin)	Sigma-Aldrich	Cat#A8806
Anakinra (Kineret®), recombinant human IL-1ra; 100 mg/0.67ml	Swedish Orphan Biovitrum AB	N/A
recombinant Mouse IL-1b/IL-1F2	R&D	Cat#401-ML-025
atropine sulfate salt monohydrate	Sigma	Cat#A0257-5G
ipratropium bromide monohydrate	Sigma	Cat#I1637-250MG
darifenacin hydrobromide	Sigma	Cat#SML-1102-50MG
murine anti-IL-1β antibody	Novartis	Cat#BSUR05, Cat#BSUR01
Critical commercial assays		
Mouse/rat insulin kit	Meso Scale Discovery	Cat#K152BZC
V-plex mouse IL-1β kit	Meso Scale Discovery	Cat#K152QPD-1
V-PLEX Human IL-1Ra individual assay kit	Meso Scale Discovery	Cat#K151WTD
Paracetamol Three Reagent System	Cambridge Life Sciences Ltd	Cat#K8002
Nucleo Spin RNA II Kit	Machery Nagel	Cat#740955.250
GoScript Reverse Transcription Mix using Random Primers	Promega	Cat#A2801
GoTaq qPCR Master Mix	Promega	Cat#A600A

(*Continued on next page*)

Continued

REAGENT or RESOURCE	SOURCE	IDENTIFIER
GoTaq Probe qPCR Master Mix	Promega	Cat#A6102
Experimental Models: Organisms/Strains		
C57BL/6NCrl *Mus musculus*	in-house breeding (originated from Charles River Germany)	MGI:2683688; Strain Code 027; RRID:IMSR_CRL:027
Il1b$^{-/-}$ (*B6;Il1b/N*)	Dror et al., 2017	N/A
Lyz2Cre-Il1b$^{fl/fl}$ (*B6.Cg-Lyz2/N x B6-IL1b/N*)	Dror et al., 2017	N/A
Cx3cr1CreER-Tak1$^{fl/fl}$ (*B6.Cg-Cx3cr1/J x B6.Cg-Map3k7/J*)	Goldmann et al., 2013	N/A
Cx3cr1CreER-EYFP (B6.129X1-*Gt(ROSA)26Sor*/J x B6.Cg-Cx3cr1/J)	Goldmann et al., 2013	EYFP: The Jackson Laboratory stock #006148, Cx3cr1CreER: NA
Cx3cr1CreER-Il1b$^{fl/fl}$ (*B6.Cg-Cx3cr1<tm2.1(cre/ERT2)Jung>* x *B6-Il1b<tm1Boe>/N*)	in-house breeding	N/A
Oligonucleotides		
Actb	Thermo Fisher Scientific	Cat#PN4351370; TaqMan Assay ID: Mm00607939_s1
Gapdh	Thermo Fisher Scientific	Cat#PN4351370; TaqMan Assay ID: Mm99999915_g1
Il1b	Thermo Fisher Scientific	Cat#PN4351370; TaqMan Assay ID: Mm0043228_m1
Tnf	Thermo Fisher Scientific	Cat#PN4351370; TaqMan Assay ID: Mm00443258_m1
Il1b FW: GCAACTGTTCCTGAACTCAACT; *Il1b* REV: ATCTTTTGGGGTCCGTCAACT	Microsynth	N/A
18S FW: CTCAACACGGGAAACCTCAC; *18S* REV: CGCTCCACCAACTAAGAACG	Microsynth	N/A
Ccnb2 FW: TTCTGGTGCTTGTCTCACTGA; B2 REV: CAGTATGTTCGGCTTCCCATTC	Microsynth	N/A
Ppia FW: GAGCTGTTTGCAGACAAAGTTC; *Ppia* REV: CCCTGGCACATGAATCCTGG	Microsynth	N/A
Software and algorithms		
Prism 8	Graphpad Prism	https://www.graphpad.com; RRID: SCR_002798
FlowJo 10.6.1 software	Tree Star	https://www.flowjo.com/solutions/flowjo/downloads; RRID:SCR_008520
R (version 3.6.0)	www.r-project.org	N/A
Other		
mouse chow	Kliba Nafag	Cat#3436.EX.F12
high-fat diet	ssniff Spezialitäten, Soest, Germany	Cat#EF D12492 (I) mod. 60 kJ% fat [Lard]

RESOURCE AVAILABILITY

Lead contact

Further information and requests for resources and reagents should be directed to and will be fulfilled by the lead contact, Sophia Wiedemann (sophia.j.wiedemann@gmail.com)

Materials availability

This study did not generate new unique reagents.

Data and code availability

- All data reported in this paper will be shared by the lead contact upon request. Raw data used to generate graphs are included in Data S1.

- This paper does not report original code.
- Any additional information required to reanalyze the data reported in this paper is available from the lead contact upon request.

EXPERIMENTAL MODEL AND SUBJECT DETAILS

Animals

Male and female wild-type mice (C57BL/6NCrl), Il1b$^{-/-}$ (B6N.B6-*Il1b<tm1Boe>*) and *Lyz2*-Cre *Il1b*$^{fl/fl}$ (*B6N.Cg-Lyz2<tm1(cre)Ifo>*) (Dror et al., 2017) were obtained from our in-house breeding and kept on a pure C57BL/6NCrl genetic background.

Male and female *Cx3cr1*-Cre^{ERT2} *Tak1*$^{fl/fl}$ (*B6.Cg-Cx3cr1<tm2.1(cre/ERT2)Jung> x B6.Cg-Map3k7<tm1Aki>*) (Goldmann et al., 2013) were kindly donated by Andrew Pospisilik (Max Planck Institute of Immunobiology and Epigenetics Freiburg) and kept on a C57BL/6J genetic background. To generate the *Cx3cr1*-Cre^{ERT2} *EYFP* line, B6N.129X1-*Gt(ROSA)26Sor<tm1(EYFP)Cos>* mice (JAX stock #006148; (Srinivas et al., 2001)) were crossed to B6.Cg-Cx3cr1<tm2.1(cre/ERT2)Jung> and kept on a C57BL/6J genetic background. To generate *Cx3Cr1*-Cre^{ERT2}*Il1b*$^{fl/fl}$ (*B6.Cg-Cx3cr1<tm2.1(cre/ERT2)Jung> x B6-Il1b<tm1Boe>/N*) mice *Cx3Cr1*-Cre^{ERT2} mice were backcrossed onto a C57BL/6NCrl genetic background (>10 generations) and crossed with Il1b$^{fl/fl}$ mice. For induction of Cre recombinase mice were treated with 125 mg/kg tamoxifen (#T5648, Sigma) dissolved in ethanol and corn oil (#C8267, Merck) and orally gavaged at two time points 48 h apart. For all experiments involving conditional knock-out mice, littermate controls carrying the respective loxP-flanked alleles, but not Cre-recombinase, were used as controls.

Mice for vagus nerve activity measurements were housed at the animal facility of the University of Paris, France. All other mice were housed at the SPF animal facility of the University Hospital of Basel, Switzerland under temperature-controlled conditions, in a room with a 12 h light and 12 h dark cycle with free access to chow (#3436.EX.F12, Kliba Nafag) and water, unless indicated otherwise.

All mice were between 7- and 14-weeks-old at the start of experiments, unless indicated otherwise. Littermate mice were weight-, sex- and age-matched between experimental groups, but otherwise randomly assigned to treatments. At least three independent cohorts were pooled. Experiments were performed on the same time of day to minimize differences in experimental conditions between cohorts. Whenever possible studies were done in a crossover design with a 7-day or more rest period between experiments.

All animal experiments were approved by the Swiss or French authorities and conducted according to local institutional guidelines and the Swiss animal welfare act. Wherever possible, each cage included mice receiving all treatments in order to avoid cage-dependent effects. For experiment-specific deviating housing conditions, food, husbandry and body weights, see the specific figure legends.

METHOD DETAILS

Cephalic phase experiments

Mice were fasted overnight for 14 h (6 p.m. to 8 a.m.; free access to water). Mice were then placed into a new cage with fresh bedding that was either otherwise empty (control condition) or contained a single food pellet of the chow they were accustomed to (cephalic condition). For the non-edible condition, a rubber stopper the size and shape of a single food pellet was placed into the new cage. Cephalic-stimulated mice were then allowed to voluntarily approach the food pellet. Blood was sampled immediately after the first bite of food. Control and non-edible-stimulated mice were left in the new cage for a time matching the time it took cephalic-stimulated mice to bite the food pellet. As a representative example a video of the procedure is provided (Video S1). For the timing of the behavior protocol see Figure 2A and for the dose of injected compounds, as well as the specific mouse-strains used, see the corresponding figure legends.

Glucose tolerance tests

Mice were fasted for 6 h (8 a.m. – 2 p.m.). At T=0 (2 p.m.), glucose was either injected intra-peritoneally (ipGTT) or administered by gavage (oGTT) at a final dose of 2g/kg of body weight. Cephalic-stimulated and exogenous insulin-treated oGTT mice were fasted overnight for 14 h (6 p.m to 8 a.m with free access to water). For insulin and glucose measurements, tail-vein blood was collected at the indicated timepoints. Blood glucose levels were determined using a glucometer (FreeStyle, Abbott Diabetes Care Inc.). For the timing and dose of other experiment-specific injected compounds please see the corresponding figure legends.

Fasting-refeeding experiments

Mice were fasted (free access to water) overnight for 12h (6 p.m. - 6 a.m.). At 6 a.m., mice were either kept fasted for an additional 2 h (control condition) or refed for 2 h (refed condition), and were immediately sacrificed for organ collection. Fasting and refeeding, as well as subsequent organ collection were conducted at the same time of day (8 a.m – 10 a.m) to minimize circadian-cycle-mediated fluctuations of circulating IL1β.

High-fat diet feeding experiments

Female wild-type C57BL/6NCrl mice were fed a high-fat diet (D12492, ssniff Spezialitäten, Soest, Germany; 60% fat = HFD condition) for up to 8 weeks. For repeated anti-IL-1β injection experiments, mice either received three i.p injections of anti-IL-1β or isotype control over three weeks while on HFD. The first injection of anti-IL-1β (15mg/kg) was given at the start of HFD feeding. The subsequent

second (15mg/kg) and third (7.5mg/kg) injections were given in weekly intervals. Before HFD-feeding and anti-IL-1β (or isotype control) administration, a cephalic phase experiment was performed with the mice to have the baseline measurements. After HFD-feeding and anti-IL-1β (or isotype control) administration the same mice were exhibited to a cephalic phase experiment (see Figure 6H).

Basal IL-1beta protein measurements

Mice were fasted for 6 h (8 a.m. – 2 p.m.) with free access to water. At 2 p.m. tail blood was collected for serum IL-1β protein measurements (detailed under *Protein measurement assays*).

Intracerebroventricular cannula implantation

10- to 13-week-old female wild-type C57BL/6NCrl and Il1b$^{-/-}$ mice were injected with ketamine/xylazine in saline (ketamine 65mg/kg body weight; Ketamin Labatec, Labatec Pharma SA; xylazine 12mg/kg body weight; Xylazin Streuli ad us. Vet., Streuli Pharma AG). Next, viscotears (Lacrinorm, Bausch & Lomb Swiss AG) were applied to the mice's eyes to prevent them from desiccation and the top of the skull was shaved. The mice were then fixed to the stereotactic frame (Kopf) and the skin was opened to expose the skull. The periosteum was removed with acetone and a burr hole was placed at x: -0.7mm; y:-1.3mm from bregma. Next, the guide cannula (stainless steel with a plastic pedestal, Bilaney consultants, cat#: C315GS-5/SP) was implanted at (x: -0.7mm; y:-1.3mm; z=-1.85mm (Franklin and Paxinos, 2019)), thereby targeting the lateral ventricle. Cyanoacrylate glue was used to provisionally hold the guide cannula in place. Then dental acrylic cement (Paladur, Kulzer) was built up around the cannula to definitely fix it in place. Postoperative analgesia was performed by a one-time i.p. injection of Buprenorphine (0.1mg/kg body weight; Bupaq ad us. vet., Streuli Pharma AG) immediately after surgery. Thereafter, Buprenorphin continued to be provided in the drinking water (0.3mg/ml) for a period of 3 days. Henceforth, the mice remained single-caged. All mice were allowed to recover for a minimum period of 2 weeks after surgery.

Vagus nerve activity measurements

Firing rate activities were recorded at the level of the thoracic branch of the vagus nerve (parasympathetic) in 5-hour-fasted mice, as previously described (Magnan et al., 1999). Briefly, mice were anesthetized with isoflurane (Sanofi). The vagus nerve, was dissected free of the underlying tissues to a distance of approximately 5 mm. The vagus nerve was then covered with paraffin oil to prevent dehydration and carefully placed on a pair of recording silver wire electrodes (0.6-mm diameter). Electrodes were connected to a high-impedance probe, and action potentials were displayed and saved on a computer after initial amplification through a low-noise amplifier (Bio Amp, ADInstruments, Dunedin, NZ). As the recordings were made on anesthetized animals, they were placed on a heated blanket and the rectal temperature was monitored throughout the duration of the experiment.

Unipolar nerve activity was recorded continuously for 10 min (baseline) and then 10 minutes after a single injection of either saline or IL1β (T=0, i.p., 1μg/kg body weight) followed by injection of either saline or glucose at T=5 min (i.p., 3 g/kg body weight). Data were digitized with digitizer PowerLab/4sp. Signals were amplified 10^5 and filtered at low- and high-frequency cut-offs of 100 and 1,000 Hz and monitored with the computer program Chart 4 (ADInstruments, Dunedin, NZ).

Histology and c-FOS quantification

For the cephalic phase experiments and sacrifice, wild-type i.c.v.-cannulated C57BL/6NCrl mice were fasted overnight for 14 h (6 p.m. to 8 a.m.). At T-1 h before the cephalic phase experiment (7 a.m.), they received one intracerebroventricular injection of either IL-1Ra (Kineret®; recombinant human IL-1Ra, Swedish Orphan Biovitrum AB; 25 mg/kg body weight) or solvent (10 mM sodium citrate, 140 mM NaCl, 0.5 mM EDTA, polysorbate 80 at pH 6.5, 150 mg/ml BSA in water). Immediately after the cephalic phase experiment, the mice were sacrificed in a CO_2-chamber and transcardially perfused for 1.5 min with 0.1M phosphate buffer (PB) followed by 4% paraformaldehyde in 0.1M PB (PB-PFA pH 7.4) for 2.5 min. Brains were post-fixed overnight in 4% PB-PFA and cryoprotected overnight in 20% sucrose-0.1 M PB. They were then frozen in hexane on dry ice for 3 min and stored at -80°C. Four series of 25 μm thick coronal sections across the PVH and the AP/NTS/DMV regions were cut on a cryostat and slide-mounted onto superfrost plus slides (Life Technologies Europe, Zug). Slides were stored in cryoprotectant (40% PBS-30% glycerol and 30% ethylene glycol) at -20°C. Brain sections were then processed for c-Fos imaging to quantify the number of activated neurons in the PVN and AP/NTS/DMV nuclei in response to the different treatments.

For c-FOS immunohistochemistry, blocking was performed in PBS containing 0.4% Triton X and 4% normal goat serum for 2 h at room temperature. Sections were incubated at 4°C for 48 h with anti-c-Fos primary antibody (1:500, #2250, Cell Signaling Technology) and after washing with PBS, they were then incubated with goat anti-rabbit Alexa Fluor 488 (AP/NTS/DMV; 1:200, Jackson Immunoresearch) or goat anti-rabbit CY3 (PVH; 1:200, Jackson Immunoresearch) for 2 h at room temperature. Sections were counterstained with DAPI (Life Technologies Europe, Zug, Switzerland) and coverslipped with vectashield (Vectorlabs, Servion, Switzerland) (Coester et al., 2020).

For image analysis, cells expressing c-Fos in the PVH and AP/NTS/DMV were imaged using an L2 Imager upright microscope at 20X magnification (Zeiss, Germany) at similar exposure time. Images were set to the same threshold and c-Fos-positive neurons were counted using ImageJ (NIH). Three consecutive PVH or AP/NTS/DMV sections from bregma -0.71 to -1.07 and -7.43 to -7.67 respectively (Paxinos and Franklin, 2012), as verified by DAPI counterstaining, were used for quantification and averaged.

Primary cell isolation

Mouse peripheral blood mononuclear cells (PBMCs), splenic cells, peritoneal macrophages, colonic macrophages and adipose-tissue macrophages were isolated as described in Brykczynska et al. (2020).

Myeloid cells of the liver were isolated by perfusion of the organ with 4 ml collagenase solution through the common bile duct (1.4 g/l; collagenase type 4; Worthington). The livers were then transferred into 50ml conical tubes containing collagenase solution and minced into small pieces using scissors. The tubes were incubated shaking for 30 min at 37°C. After incubation, the suspension was filtered twice. First through cotton gauze to hold back larger pieces and then through a 70-μm cell strainer (#431751, Corning). The tube containing the filtered cell sample was filled up to 50 ml with FACS buffer (PBS with 0.5% BSA and 5 mM EDTA) and centrifuged for 3 min at 40 *g*. The supernatant was transferred into a fresh 50 ml conical tube and the pellet was resuspended again and filled up to 50 ml with FACS buffer and centrifuged for 3 min at 30 *g*. The supernatant was transferred into a clean conical tube and the pellet was discarded. The two supernatants were centrifuged for 5 min at 350 *g*. The pellets were resuspended, pooled together and resuspended in a 37% isotonic Percoll solution (#17-0891-01, GE Healthcare). The 37% Percoll-cell-solution was then layered on top of a 70% isotonic Percoll solution and centrifuged for 30 min at 500 *g* using minimal brake. The myeloid-cell containing interphase was then collected and once again filtered through a 70-μm cell strainer (#431751, Corning), washed and resuspended in FACS buffer for further FACS analysis.

Microglia were isolated following a protocol adapted from Brykczynska et al. (2020), with the following change: For mechanical dissociation, dissection medium (HBSS (GIBCO without $CaCl_2$ and $MgCl_2$) with 15 mM HEPES and 1.3% glucose) rather than FACS-buffer was used. For knock-out efficiency testing *Cx3cr1-Cre^{ERT2} Il1bflx* mice and their Cre-negative littermates were stimulated with two administrations of LPS before sacrifice; LPS (1mg/kg) i.p injections 24 h and 3 h before sacrifice.

Islet macrophages were isolated and dispersed as described in Dalmas et al. (2017). Pancreata were perfused through the common bile duct with 2ml of HBSS collagenase solution (GIBCO, 1.4g/l; collagenase type 4; Worthington) and transferred to 50ml tubes containing the same solution. After incubating in a 37°C water bath for 28 min, samples were homogenized by vigorous shaking and washed three times with HBSS supplemented with 0.5% BSA. Next, samples were first filtered through a 500μm mesh and then through an inverted 70μm (#431751, Corning) cell strainer. Islet were retained on the 70μm (#431751, Corning) cell strainer and transferred to petri dishes containing RPMI-1640 (GIBCO) supplemented with 11.1mM glucose 100 units/ml penicillin, 100μg/ml streptomycin, 2mM Glutamax, 50μg/ml gentamycin, 10μg/ml Fungison and 10% FBS (Invitrogen). Isolated islets were kept in supplemented RPMI-1640 solution at 37°C and 5% CO_2 until further processed. To obtain single cell suspension, islets were gently dispersed with a 0.0125% trypsin-EDTA (GIBCO) solution for 2 min in a 37°C water bath. After washing with cold FACS buffer and centrifuging the dispersed cells at 300 *g*, 4°C for 5 min, the cells were recovered in cold FACS buffer.

RNA-extraction and qPCR

We extracted total RNA with the Nucleo Spin RNA II Kit (Machery Nagel). RNA concentrations were then normalized and the RNA reverse-transcribed with the GoScript Reverse Transcription Mix using Random Primers (#A2801 GoScript, Promega) according to the manufacturer's instructions. SYBR Green assays with GoTaq qPCR Master Mix (#A600A, Promega) or TaqMan assays with GoTaq Probe qPCR Master Mix (#A6102, Promega) were used to determine mRNA expression with the ViiA 7 Real-Time PCR System (ThermoFisher Scientific). Primers for SYBR Green-based and TaqMan qPCR can be found in the key resources table. The data were normalized to the geometrical mean of *Actb* and *Gapdh* (Figure 4G), *18S* or *Ccnb2* and *Ppia* (Figure 4H) or *Actb, 18S* and *Ppia* (Figure 4L) values and analyzed using the comparative $2^{-\Delta\Delta CT}$-method.

Flow cytometry

Isolated cells were incubated with an anti-mouse CD16/CD32 antibody (clone 93, #14-0161-85, eBioscience) for 15 min at room temperature in the dark and subsequently labeled with the panel-appropriate antibodies for 30 min at 4°C in the dark. For islet macrophages, peritoneal macrophages, adipose tissue macrophages and colonic macrophages we used: APC anti-mouse CD45 [clone 30-F11] (#17-0451-83, eBioscience), PE anti-mouse CD11b [clone M1/70] (#12-0112-81, eBioscience) and PECy7 anti-mouse F4/80 [clone BM8] (#25-4801-82, eBioscience). In case of liver macrophages, the same panel as for islet macrophages was used with the addition of PE-Cy5 anti-mouse MHC-II [clone M5/114.15.2] (#107612, BioLegend). In case of monocytes, the following antibodies were used: APC anti-mouse CD115 [clone AFS98] (#17-1152-82, eBioscience), PerCP-Cyanine5.5 anti-mouse Ly6C [clone HK1.4] (#45-5932-82, eBioscience) and APC-Cy7 anti-mouse Ly6G [clone 1A8] (#127624, BioLegend). For microglia, we used PerCP-Cyanine5.5 anti-mouse Ly6C [clone HK1.4] (#45-5932-82, eBioscience), APC-Cy7 anti-mouse Ly6G [clone 1A8] (#127624, BioLegend) (or an APC-Fire750-conjugated antibody of the same clone (#127651, BioLegend)), Super Bright 600 anti-mouse CD45 [clone 30-F11] (#63-0451-82, eBioscience), APC anti-mouse P2RY12 [clone S16007D] (#848006, BioLegend), PE anti-mouse CD206 [clone MR6F3] (#12-2061-82, eBioscience) and PE-Texas Red anti-mouse CD11b [clone M1/70.15] (#RM2817, eBioscience). For splenic as well as peripheral blood B-cells, CD8-T-cells and CD4-T-cells we used the following panel: Super Bright 600 anti-mouse CD45 [clone 30-F11] (#63-0451-82, eBioscience), APC-Cy7 anti-mouse CD3e [clone 145-2C11] (#100330, BioLegend), PE-Cy7 anti-mouse B220 [clone RA3-682] (#25-0452, eBioscience) (or an PerCP-eFluor710-conjugated antibody of the same clone (#46-0452, eBioscience)), PE anti-mouse CD4 [clone GK1.5] (#12-0041-81, eBioscience) and APC anti-mouse CD8a [clone 53-6.7] (#17-0081-81, eBioscience). Appropriately stained cells were then washed twice with FACS buffer and stained for viability with the DNA-binding dye DAPI (#422801, BioLegend), before sorting/analyzing of the final cell populations on a BD FACS-Aria III or a Beckman Coulter CytoFLEX, respectively. Gating was performed uniquely on the basis of fluorescence minus one (FMO) control. The

different cellular populations were defined as follows: microglia: DAPI- single CD45intCD11b+P2RY12+CD206-Ly6C-Ly6G-. Of note, for microglia we first used a simplified panel, where we only identified them on the basis of DAPI- single CD45intCD11b+Ly6C- (same antibodies as used for the islet macrophage panel above, plus PerCP-Cyanine5.5 anti-mouse Ly6C [clone HK1.4] (#45-5932-82, eBioscience)). We then repeated these experiments with the more specific panel for better resolution of the cellular populations in the brain. The results were highly similar and thus pooled for the final graph. Ly6C-high monocytes: DAPI- single CD115+ Ly6G- Ly6C+. Ly6C-low monocytes: DAPI- single CD115+ Ly6G- Ly6C-. Islet macrophages, peritoneal macrophages, adipose tissue macrophages and colonic macrophages: DAPI- single CD45+ CD11b+ F4/80+. Liver macrophages: DAPI- single CD45+ CD11b+ MHC-II+. B-cells, CD8-T-cells and CD4-T-cells of the spleen and peripheral blood: DAPI- single CD45+CD3-B220+, DAPI- single CD45+CD3+B220-CD8+ and DAPI- single CD45+CD3+B220-CD4+ respectively. For representative examples of the respective gating strategies, please see Figures 4L and S3.

Protein measurement assays

Insulin levels were determined with the mouse/rat insulin kit (#K152BZC-1 Meso Scale Discovery). Mouse IL-1β concentrations were analyzed using the V-plex mouse IL-1β kit from Meso Scale Discovery (#K152QPD-1, alternate protocol 1, extended incubation). Human IL-1Ra measurements were performed using the V-PLEX Human IL-1Ra individual assay kit (#K151WTD, Meso Scale Discovery). Paracetamol measurements were performed with the Paracetamol Three Reagent System (#K8002, Cambridge Life Sciences Ltd).

QUANTIFICATION AND STATISTICAL ANALYSIS

General information

Biostatistics analysis were performed using GraphPad Prism (version 8 and 9) software (GraphPad, Inc, La Jolla, CA). Specific statistical tests employed, statistical parameters (reported measures of dispersion and summary measures) and numbers of replicates can be found in the figures and figure legends. Statistical assumptions were tested beforehand and either found to be met or the statistical test was exchanged for a procedure that better fit the data.

Meta-analysis

The secondary analysis of our recently published meta-analysis (Wiedemann et al., 2020) comparing studies assessing cephalic phase insulin secretion in lean versus obese individuals, was pre-specified in the PROSPERO protocol (see CRD42019124149). For the details of the overall meta-analysis, please see the publication (Wiedemann et al., 2020). Using the data extracted in Wiedemann et. al., we performed a Random-Effects Meta-analysis of the standardized mean difference across trials with an added moderator for the body weight of the study population (lean defined as mean BMI < 30 kg/m^2, obese ≥ 30 kg/m^2), applying the residual maximum likelihood method and Hartung-Knapp adjustment. Notably, of the 37 reports (comprising 77 studies) identified by the meta-analysis, a total of 9 studies described results taken from patient populations with a bmi ≥ 30 kg/m^2 (termed obese). Those 9 studies assessed 86 participants in total. The 68 studies describing ''lean'' patient populations (bmi < 30 kg/m^2) assessed a total of 662 participants.

ADDITIONAL RESOURCES

The secondary analysis of the meta-analysis previously published by Wiedemann et al. (2020) has been pre-registered on PROSPERO (CRD42019124149). For the details of the pre-specified protocol, please see: ''*PROSPERO protocol:https://www.crd.york.ac.uk/prospero/display_record.php?RecordID=124149*''. For the manuscript of the meta-analysis see: ''*meta-analysis:* https://www.sciencedirect.com/science/article/pii/S0195666320300192?via%3Dihub''.